Palaeontology
The Palaeontological Association
www.palass.org

[Palaeontology, 2022, e12631]

How long does a brachiopod shell last on a seafloor? Modern mid-bathyal environments as taphonomic analogues of continental shelves prior to the Mesozoic Marine Revolution

by ADAM TOMAŠOVÝCH[1,*], DIEGO A. GARCÍA-RAMOS[2], RAFAŁ NAWROT[3], JAMES H. NEBELSICK[4] *and* MARTIN ZUSCHIN[3]

[1]Slovak Academy of Sciences, Earth Science Institute, Bratislava 84005, Slovakia; geoltoma@savba.sk
[2]Dipartamento di Fisica e Scienze della Terra, Università degli Studi di Ferrara, Via Saragat 1, 44122 Ferrara, Italy
[3]Department of Palaeontology, University of Vienna, Josef-Holaubek-Platz 2, 1090 Vienna, Austria
[4]Department of Geosciences, University of Tübingen, Schnarrenbergstrasse 94-96, 72076 Tübingen, Germany
*Corresponding author

Typescript received 21 April 2022; accepted in revised form 30 August 2022

Abstract: Carbonate skeletal remains are altered and disintegrate at yearly to decadal scales in present-day shallow-marine environments with intense bioerosion and dissolution. Present-day brachiopod death assemblages are invariably characterized by poor preservation on continental shelves, and abundant articulated shells of brachiopods with complete brachidia are thus not expected to be preserved if not rapidly buried. However, such preservation is paradoxically observed in shallow-water Palaeozoic and Mesozoic brachiopod assemblages. Here, we show that a bathyal death assemblage time-averaged to several millennia (Adriatic Sea) consists of sediment-filled articulated shells of *Gryphus vitreus* with complete brachidia. Post-mortem age distributions indicate that disintegration half-lives exceed several centuries (*c.* 500–1700 years). The high frequency of articulated but centuries-old shells (>50%) and the fitting of taphonomic models to post-mortem ages indicate that disarticulation half-life is unusually long (*c.* 200 years). Rapid sediment filling of shells: (1) inhibited disarticulation, loop fragmentation and colonization by coelobites; and (2) induced precipitation of ferromanganese oxides at redox fronts within shells. Sediment-filled articulated shells, however, still resided at the sediment–water interface as indicated by encrusters and sponges that infested them after death. Sediment-filled shells disintegrated through bioerosion and physical wear when residence in the taphonomically active zone exceeded *c.* 2000 years. We suggest that the articulation paradox is driven by the Mesozoic Marine Revolution (MMR) that escalated predation, bioturbation and organic matter recycling, all intensifying shell disintegration. A scenario with slow disarticulation in bathyal environments may have lead to preservation of articulated shells in shallow-water assemblages prior to the MMR.

Key words: Brachiopoda, time averaging, taphonomy, Mesozoic Marine Revolution, Adriatic Sea, disarticulation.

CARBONATE skeletal remains are altered and degrade rapidly in the taphonomically active zone (TAZ) of present-day continental shelves, typically at yearly to decadal scales (Davies *et al.* 1989; Kidwell *et al.* 2005; Tomašových *et al.* 2014, 2016*a*; Olszewski & Kaufman 2015; Ritter *et al.* 2017; Albano *et al.* 2020). This dynamic is expressed by destructive alteration (here, modification of skeletal remains that does not lead to the loss of taxonomic identifiability) and final disintegration to unidentifiable remains directly observed in laboratory or natural conditions (Glover & Kidwell 1993; Powell *et al.* 2011*a*; Pace *et al.* 2020; Ashton-Alcox *et al.* 2021), time series of species abundance in living and death assemblages (DAs) (Cummins *et al.* 1986; Powell 1992; Powell *et al.* 2006), and distributions of post-mortem shell ages measured in the upper decimetres of modern seabeds (Flessa *et al.* 1993; Kosnik *et al.* 2007, 2009; Dexter *et al.* 2014). Most Holocene and Anthropocene brachiopod DAs in shelf environments are thus represented by disarticulated and fragmented valves (Noble & Logan 1981; Llompart 1988; Emig 1990; Carroll *et al.* 2003; Tomašových 2004; Simões *et al.* 2007*a*, 2007*b*; Krause *et al.* 2010; Rodrigues & Simões 2010). High abundance of articulated shells of brachiopods with fragile lophophore supports, without any obvious signs of rapid burial, however, is typical of level-bottom mudrocks, thin shell beds or biostromes in the Palaeozoic and Mesozoic stratigraphic record (Copper 1997; Feldman 2005; Chen

et al. 2010; Tessitore *et al.* 2013; Abdelhady & Fürsich 2014). A transient burial of skeletal remains by sediment veneers or by deeper stochastic burial induced by burrowers can temporarily delay disarticulation (Olszewski 1999; Parsons-Hubbard *et al.* 1999; Cherns *et al.* 2008; Dattilo *et al.* 2008, 2012; Tomašových *et al.* 2014; Nawrot *et al.* 2022). To preserve articulated shells with delicate lophophore supports in the stratigraphic record, however, this burial effect is still conditioned by the lack of subsequent mixing or dissolution induced by bioirrigation in the mixed layer and/or by the lack of durophagous predation (Walker *et al.* 2002; Cherns & Wright 2009). DAs with high abundance of articulated elements of epifaunal species deposited under slow sedimentation, as documented in the pre-Cenozoic stratigraphic record (Heliasz & Racki 1980; Fürsich *et al.* 2001; Zonneveld 2001), thus do not seem to have any clear taphonomic analogues in present-day shelf (non-deltaic) environments.

The increase in the thickness of shell accumulations towards thick and internally-complex, modern-type shell beds dominated by molluscs began during the Jurassic and generally coincides with the Mesozoic Marine Revolution (MMR; Kidwell & Brenchley 1996; Simões *et al.* 2000). This trend is accompanied by an increase in alteration of skeletal remains (Kidwell 1990; Bambach 1993; Kidwell & Brenchley 1994, 1996). The MMR that accelerated the evolution of burrowers, borers, grazers and predators, led to the displacement of poorly mobile (mainly epifaunal) groups with low-energy life strategies by mobile (especially infaunal) groups that intensified sediment mixing and irrigation, in association with diversification of several planktonic groups (Thayer 1983; Walker & Brett 2002; Clapham *et al.* 2006; Tomašových 2008; Gorzelak *et al.* 2012; Buatois *et al.* 2016; Martin & Servais 2020; Petsios *et al.* 2021). Although the onset of the MMR can vary depending on the type of ecosystem function (Buatois *et al.* 2022; Fantasia *et al.* 2022), it can be hypothesized that the restructuring of marine ecosystems also increased the overall disarticulation, fragmentation and other sources of alteration of skeletal remains as the recycling of carbonate and organic matter intensified and shell-destroying biological agents evolved through time. The processes inducing this shift may thus also be responsible for the lack of analogous conditions leading to preservation of delicate traits in present-day surface DAs.

We hypothesize that the taphonomic analogues of preservation pathways with slower rates of alteration typical for continental shelves prior to the MMR can still occur today at bathyal depths, where biomixing, bioirrigation or bioerosion tend be less intensive owing to limited light penetration, reduced organic flux and decreased benthic biomass production (Boudreau 1994; Middelburg *et al.* 1997). For example, multiple studies documented high abundance of subfossil cold-water coral assemblages of Pleistocene or Early Holocene age in bathyal environments in the Mediterranean, Atlantic or Pacific oceans (Thiagarajan *et al.* 2013; Margolin *et al.* 2014; Pratt *et al.* 2019), sometimes even 500–1000 m below the aragonite saturation horizon (Thresher *et al.* 2011*a*, 2011*b*), indicating that such remains can endure long residence in the TAZ at bathyal depths. Present-day bathyal environments may thus be characterized by slower disintegration of carbonate remains relative to conditions on continental shelves affected by high predation pressure and by intense organic carbon respiration, bioturbation and bioirrigation (Walter *et al.* 1993; Walker *et al.* 1998; Callender *et al.* 2002; Powell *et al.* 2011*b*), and can better represent taphonomic pathways near the sediment–water interface prior to the MMR. Anthropogenic impacts that have perturbed marine benthic ecosystems during the past decades or centuries, decreasing bioturbation and enhancing the stratigraphic resolution of DAs on continental shelves (Tomašových *et al.* 2018, 2020), may also resurrect pathways that are characterized by limited intensity of alteration and disintegration processes in the TAZ. Such Anthropocene changes in taphonomic pathways, however, were documented in infaunal-dominated, prodeltaic habitats with high sedimentation rates rather than in epifaunal communities subjected to slow sedimentation (Tomašových *et al.* 2021).

Here, we focus on the preservation of the epifaunal brachiopod *Gryphus vitreus* in the middle bathyal (580 m) of the Bari Canyon in the Adriatic Sea (Fig. 1). *Gryphus vitreus* shells in surface DAs disarticulate and disintegrate at a high rate at shallower depths (on the shelf edge and in the upper bathyal depths at 100–300 m) in the western Mediterranean Sea, leading to rarity or absence of articulated shells (Caulet 1972; Llompart 1988; Emig 1990). The DA collected in this study in the Bari Canyon, however, represents a major departure from the preservation style typical for the shallower DAs because, as our analyses show, well-preserved articulated shells of *G. vitreus* are both abundant and very old (>500 years) here. In a companion study based on the distribution of post-mortem ages of *G. vitreus* measured at this site, we inferred that this species attained higher population density in the Bari Canyon in the past, with abundance pulses occurring at *c.* 550 and 1750 years BP (Tomašových *et al.* 2022*a*).

In this study, to assess the discrepancy in brachiopod preservation between shelf and bathyal environments, we: (1) evaluate pathways that led to the formation of this DA by combining age, size and taphonomic data; and (2) attempt to estimate disarticulation half-lives of brachiopod shells in the TAZ. We argue that the preservation of articulated brachiopod shells in the Bari Canyon is not a signature of limited time averaging but is rather a unique indicator of the low intensity of alteration and

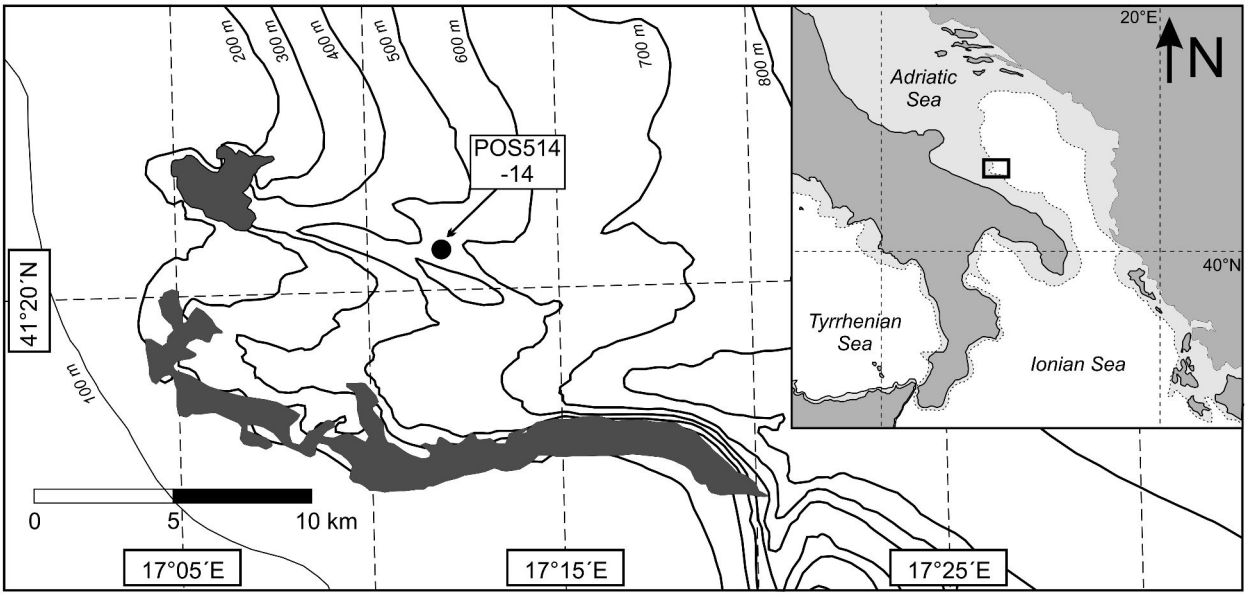

FIG. 1. Geographic map of the Bari Canyon, with the location of station POS514-14 investigated in this study (black circle) in the southern Adriatic Sea. The sampling station is situated on the northern edge of the northern channel of the Bari Canyon (modified according to Trincardi *et al.* 2007*a*; Angeletti *et al.* 2020; Tomašových *et al.* 2022*a*). The grey-shaded areas mark the location of epibenthic communities with corals, sponges and serpulids as mapped by Angeletti *et al.* (2020).

destructive processes in the TAZ. Assemblage-level preservation states are thus not only informative about the incompleteness and the magnitude of biases of the fossil record, but also about the efficiency of ecosystem processes that directly or indirectly lead to recycling of carbonates and organic matter. We suggest that assemblages in bathyal environments of the Bari Canyon may be analogues for taphonomic conditions (not associated with episodic burial) on continental shelves prior to the onset of the MMR.

GEOLOGICAL SETTING

Sedimentation in the Bari Canyon is affected by thermohaline, cascading bottom currents of the North Adriatic Dense Water that advect sediment, organic detritus and suspended food particles downslope. These currents interact with the complex topography of the Bari Canyon, leading to a mosaic of non-depositional and depositional conditions (Ridente *et al.* 2007; Trincardi *et al.* 2007*a*, 2007*b*; Turchetto *et al.* 2007; Verdicchio *et al.* 2007; Tesi *et al.* 2008). The slopes and flanks of the Bari Canyon are inhabited by cold-water colonial and solitary corals that form three-dimensional structures (up to 80 cm high) at 305–650 m (d'Onghia *et al.* 2015; Taviani *et al.* 2016) in association with serpulids (Sanfilippo *et al.* 2013) and large sponges (Angeletti *et al.* 2020).

Mixtures of autochthonous and reworked Holocene and Pleistocene remains of corals and other invertebrates occur on the seafloor of the Bari Canyon. Dead corals of *Madrepora*, *Lophelia*, and *Desmophyllum* occurring at *c.* 250–585 m water depth vary in post-mortem age between 230 and 5100 years BP (Taviani *et al.* 2019). Molluscan DAs with a high frequency of bored and encrusted skeletal remains that occur at 200–300 m water depth, consist of Holocene and Pleistocene species (Panetta *et al.* 2013), as indicated by calibrated ^{14}C ages of two *Pseudamussium septemradiatum* specimens dated to 19 000 ± 370 and 15 350 ± 250 years BP (Colantoni *et al.* 1975; Colantoni & Gallignani 1978, Taviani 1978). The northwest slope of the South Adriatic Pit with current-generated sand waves contains benthic foraminifers transported from the inner shelf (*Ammonia*, *Elphidium*, epiphytic species; Tesi *et al.* 2017). Dead shells of *G. vitreus* were collected in surface DAs between 318–616 m in former surveys (Trincardi *et al.* 2007*a*, 2011). Dead-only *G. vitreus* shells were also collected by Van Veen grabs during the Poseidon cruise in 2017 (station POS514-14) at 580 m in the Bari Canyon and are analysed here.

Gryphus vitreus is abundant in level-bottom benthic communities inhabiting detritic, mixed-bottom, shelf-edge or bathyal habitats of the Mediterranean Sea, at depths exceeding 100 m (d'Hondt 1984; Emig 1985, 1987, 1989; Cartes *et al.* 2009; Grinyó *et al.* 2018; Rosso *et al.* 2010). Former surveys in the southern Adriatic Sea documented several occurrences of live-collected *G. vitreus* at bathyal depths between 300 and 1140 m in the nineteenth century (Sturany 1896) and in the twentieth century (Gamulin-

Brida 1973, 1983; Marano *et al.* 1989; Šimunović 1997). This species presently does not form any dense aggregations in the South Adriatic Pit, and several more recent surveys did not detect this species alive (Angeletti *et al.* 2014, 2020; d'Onghia *et al.* 2015).

Gryphus vitreus is a pedunculate, suspension-feeding brachiopod, with a smooth, punctate shell achieving 30–40 mm length (Boullier *et al.* 1986). It possesses a cyrtomatodont hinge characterized by interlocking teeth and sockets. Disarticulation of articulated valves with such a hinge entails breakage of the sockets (Sheehan 1978; Carlson 1989; Alexander 1990; Alexander & Gibson 1993). In contrast to most rhynchonelliformean brachiopods with two shell layers (represented by the outer, very thin cryptocrystalline primary layer and the inner, thicker secondary layer consisting of fibres), the posterior and central segments of *G. vitreus* valves are mainly formed by the prismatic tertiary layer (Gaspard *et al.* 2007; Allmen *et al.* 2010; Gaspard 2011). The posterior and central segments with the tertiary layer are also thicker (1 mm) than the anterior margins which lack this layer (0.3–0.5 mm). The tertiary layer is less rich in organics and thus more robust against disintegration compared to the outer, organic-rich primary and secondary layers (Gaspard 1989; Emig 1990).

MATERIAL AND METHOD

The station POS514-14 is located at 580 m water depth (41.35002 N, 17.19997E) on the northern slope of the northern branch of the Bari Canyon (Channel B in Trincardi *et al.* 2007*a*; Angeletti *et al.* 2014), consisting of mixed sandy and muddy bottom sediments (Prampolini *et al.* 2021), close to a steep, almost vertical wall of the canyon channel. At these depths, the canyon is bathed by high-density currents of the North Adriatic Dense Water, salinity is 38.8 psu and bottom-water temperature is 13.6–13.8°C (Trincardi *et al.* 2007*b*). Three grabs (numbered 5, 6, and 7) were sieved at 1 mm. All contained dead shells of *G. vitreus*, with no individuals of this species collected alive. All of the *G. vitreus* specimens (n = 59) larger than 20 mm were picked from grab 6 (labelled POS514-14-6) during the wet-sieving on board, and an additional 33 specimens larger than 3 mm were exhaustively picked from the 1/8 of the grab. 92 specimens were dated with ^{14}C, using direct carbonate accelerator mass spectrometry (Bush *et al.* 2013). ^{14}C ages were calibrated to calendar ages by using the Marine13 database, with the ΔR = 121 years based on *Mimachlamys varia* (M. Taviani & A. Correggiari, in Reimer & McCormac 2002), with details provided in Tomašových *et al.* (2022*a*). Age errors (one standard deviation) of calibrated ages attain *c.* 50 years for shells <1000 years BP and *c.* 80–90 years for shells that are *c.* 1000–3000 years old. In this study, 261 specimens (including the 92 dated specimens) exhaustively picked from grab 6 (specimens above 2 mm) were scored according to 15 taphonomic variables under reflected and transmitted light at 10–20× magnification (Table 1). These variables are scaled between 0 (pristine) and 1 (altered). The frequency of disarticulation per grab is standardized relative to the total number of complete individuals (i.e. the total number of shells plus half of disarticulated valves). All other per grab frequencies of other types of alteration are standardized relative to the sum of all specimens: the total number of shells and all disarticulated valves. In addition to the 15 variables scored on all specimens, the brachidia (the so-called loops in terebratulids) in dorsal valves were scored as absent (coded as 1) when crural processes were broken or when hinge plates were preserved only, or as present (complete loops coded as 0).

To compare the preservation of articulated shells with disarticulated valves, and to contrast the preservation of internal with external valve surfaces, we computed means of per-specimen alteration (PSA) states based on 15 variables with bootstrapped 95% confidence intervals. We assess the variation in preservation among all the specimens in principal co-ordinates analysis (PCoA), using the Manhattan distance based on their PSA (equivalent to frequency of alteration in variables with binary coding). The size of specimens was measured along the length axis of the ventral valve. The length was either directly measured on complete specimens or estimated by reduced major axis regressions for incomplete specimens based on pairwise allometric relationships between the ventral valve length and: (1) the ventral valve width; (2) the dorsal valve length; or (3) the cardinalia width when valves were incomplete.

We assess the relation between preservation on the one hand and post-mortem age and size (prior to fragmentation) on the other with: (1) non-binned; and (2) binned age and size data. First, log-transformed post-mortem ages and log-transformed lengths of specimens are used as continuous predictor variables in constrained analyses of principal co-ordinates (CAP, with the Manhattan distance). Second, in analyses of size-selectivity of preservation, size data are binned to eight 5 mm-classes. Third, in the analyses of the taphonomic clock, post-mortem age data are binned to eight age cohorts (<100 years, >100–300 years, >300–500 years, >500–1000 years, >1000–1500 years, >1500–2000 years, >5000–25 000 years, and >5000 years). Rank correlations based on the cohort-level preservation can be of borderline significance if adjusted for multiple testing with the Bonferroni correction but as the sample sizes are limited (n = 8 both in analyses of size-selectivity and taphonomic clock) and the pairwise tests between age and preservation are not independent, we report the effect size (correlation coefficients) with raw p-values.

TABLE 1. Summary of 15 taphonomic variables, scored on all individuals of *G. vitreus* larger than 3 mm.

Variable	Description and source (SEM, EDS)	Scoring
Disarticulation	Ventral and dorsal valve interlocked	0 – articulated shells 1 – valves
Fragmentation	Valve breakage, loss of outline	0 – complete outline 0.25 – chipped margins 0.5 – 50–75% preserved 0.75 – 25–50% preserved
Discolouration	Brownish and greyish colour (clay coatings and micrite cement)	0 – semitransparent or white 0.5 – patchy discolouration 1 – extensive discolouration
External encrustation	Encrusters or their attachment bases	0 – absent 0.5 – rare 1 – highly encrusted
Internal encrustation	Encrusters or their attachment bases	0 – absent 0.5 – rare 1 – highly encrusted
External microbioerosion	Borings with diameters <50 μm (mainly *Novodendrina*, anomiid scars)	0 – absent 0.5 – rare 1 – highly microbioeroded
Internal microbioerosion	Borings with diameters <50 μm	0 – absent 0.5 – rare 1 – highly microbioeroded
External macrobioerosion	Diameter exceeding 0.05–0.1 mm (*Entobia*)	0 – absent 0.5 – rare 1 – highly macrobioeroded
Internal macrobioerosion	Diameter exceeding 0.05–0.1 mm (*Entobia*)	0 – absent 0.5 – rare 1 – highly macrobioeroded
External abrasion	Rounding of valve margins, surficial wear, growth lines invisible	0 – absent 0.5 – rare 1 – highly abraded
Internal abrasion	Loss of hinge plates, teeth and sockets	0 – absent 0.5 – rare 1 – highly abraded
External rusty or ochreous coatings	Coatings, punctal and boring infills by Fe-oxide tufts	0 – absent 0.5 – dispersed mm-scale spots 1 – patches or continuous coatings > few mm
Internal rusty or ochreous coatings	Coatings, punctal and boring infills by Fe-oxide tufts	0 – absent 0.5 – dispersed mm-scale spots 1 – patches or continuous coatings > few mm
External black coatings	Coatings, punctal and boring infills by Mn-oxide globules	0 – absent 0.5 – dispersed mm-scale spots 1 – patches or continuous coatings > few mm
Internal black coatings	Coatings, punctal and boring infills by Mn-oxide globules	0 – absent 0.5 – dispersed mm-scale spots 1 – patches or continuous coatings > few mm

We inspected the preservation of internal surfaces, formed either by secondary fibres or by tertiary prisms under the scanning electron microscope (SEM) at 1000–3000× magnification. We assessed the composition of cements, surficial coatings and boring infills with the qualitative energy-dispersive x-ray spectroscopy (EDS; software INCA), with gold-coated samples. We distinguish coatings mainly formed by Fe oxides from those formed by Mn oxides on the basis of their colour because EDS analyses consistently show that black coatings are formed by Mn oxides and orange and reddish coatings by Fe oxides.

Direct estimation of disintegration (mean time it takes to disintegrate brachiopod shells to remains that cannot be identified to species level) or disarticulation rate (mean time to disarticulate brachiopod shells to individual

valves) in the TAZ is difficult when age distributions are produced by temporally-variable populations. As the frequency distribution of post-mortem ages of *G. vitreus* is bimodal, we use a model that assumes that population size of *G. vitreus* declined abruptly to zero at 450 years BP (i.e. production of dead shells that enter a DA abruptly stopped at this time) (we note that although we report ages in BP in the text, the fit is performed on post-mortem ages re-scaled relative to the time of sampling in 2017), and fit the distribution of ages of articulated shells with a simple taphonomic model to estimate disarticulation rate and half-life, assuming that the rate of disarticulation of shells does not significantly change with post-mortem age. This approach also assumes that the input of dead brachiopods remains is temporally in steady state prior to 450 years BP. Although this assumption is difficult to verify, the estimates of disintegration rates may be robust to violations of constant population size if that population does not increase or decrease over a duration corresponding to the disintegration half-life (Tomašových *et al.* 2016*a*). The estimate of disarticulation rate can be used to predict the initial number of shells that entered the sediment (the area of *c.* 0.1 m^2 sampled by a single Van Veen grab). The expected number of such shells is computed by dividing the empirical number of articulated shells in 100-year cohorts by $e^{-(\log(2)/\text{half–life}) \times \text{age}}$. This estimate of the initial number of shells is also informative about the minimum half-life because the maximum densities of *G. vitreus* or other articulated brachiopods of similar size generally do not exceed *c.* 1000 individuals/m^2 (Emig 1987). To assess size-dependency of disintegration, we assessed the overall disintegration rate of specimens (both shells and valves) smaller and larger than 20 mm (ventral valve length of individuals prior to their fragmentation as estimated from reduced major axis regressions; the threshold used here to approximately separate adult specimens from juveniles; Boullier *et al.* 1986), using the same procedure with abrupt termination in brachiopod production as used in the estimation of disarticulation rate. All age and taphonomic data are available in Tomašových *et al.* (2022*b*). All specimens from grab 6 are deposited in the collections of the Department of Palaeontology, University of Vienna.

RESULTS

Assemblage composition

DAs in all three grabs are rich in skeletal sand and gravel, with abundant benthic molluscs, pteropods, brachiopods, polychaetes (brownish-stained fragments of *Ditrupa*), foraminifers, bryozoans, and decapod fragments, and in brownish or grey, rounded, gravel-sized carbonate intraclasts (up to 5 mm). The fragments of *Pseudamussium* are worn, iron-stained (brownish colours), bored and encrusted, similarly as microbored and encrusted *Ditrupa* tubes. In contrast, the aragonitic bivalves *Abra longicallus* and *Kelliella miliaris* are represented by well-preserved, semitransparent or white, frequently complete valves. Arcid bivalves (*Bathyarca pectunculoides*, *Asperarca nodulosa*) are represented by a mixture of well-preserved, transparent to semitransparent or white valves and poorly-preserved and discoloured valve fragments with brownish, grey or orange stains. Intraclasts are microbored and encrusted with agglutinated foraminifers (e.g. *Placopsilina*, *Sagenina*, and others).

Time-averaging

The frequency distribution of post-mortem ages of *G. vitreus* is bimodal, with two modes at *c.* 500 and 1750 years BP (Fig. 2A, B). Out of 92 specimens, the calibrated ages

FIG. 2. A–B, frequency distribution of post-mortem ages (BP) of *G. vitreus* in grab sample POS514-14-6, with modes at *c.* 500 years and 1750 years, highlighting the contribution of: A, articulated shells; B, individuals >20 mm in length (estimated as the ventral valve length prior to fragmentation; the two modes are captured by both articulated and disarticulated specimens, although the contribution of articulated shells diminishes in older cohorts; both small and large specimens contribute to both modes. C, size distribution of all specimens collected in the grab 6, with articulated shells corresponding mainly to larger specimens >25–30 mm in length. D, size distribution of age-dated specimens shows that the dated subset closely captures the mode formed by adults >20 mm in length. E, the fit of the simple taphonomic model to ages of articulated shells, assuming that an abrupt offset in production (abundance of living individuals) occurred at 450 years BP, indicates that disarticulation rate is 0.0036 $year^{-1}$, half-life is *c.* 200 years. F, the expected number of initial shells computed by dividing the empirical number of articulated shells in 100-year cohorts by $e^{-(\log(2)/\text{half–life}) \times \text{age}}$; the initial number of articulated shells entering 0.1 m^2 of the sediment (area captured by a single Van Veen grab) within a 100 year period is higher than 1000 individuals for cohorts older than 1000 years; when scaled to 1 m^2, assuming a lifespan of 10 years, these values along the *y*-axis represent annual densities of *G. vitreus* expected under three disarticulation half-lives; the dashed horizontal line represents 1000 individuals; age cohorts without any shells were assigned the value of one individual in this computation. G–H, age distributions of individuals smaller and larger than 20 mm (ventral valve length of individuals prior to their fragmentation), fitted with the simple taphonomic model, assuming that an abrupt offset in production occurred at 450 years BP, indicate that disintegration rate of individuals <20 mm is 0.0013 $year^{-1}$and disintegration rate of individuals >20 mm is 0.00041 $year^{-1}$.

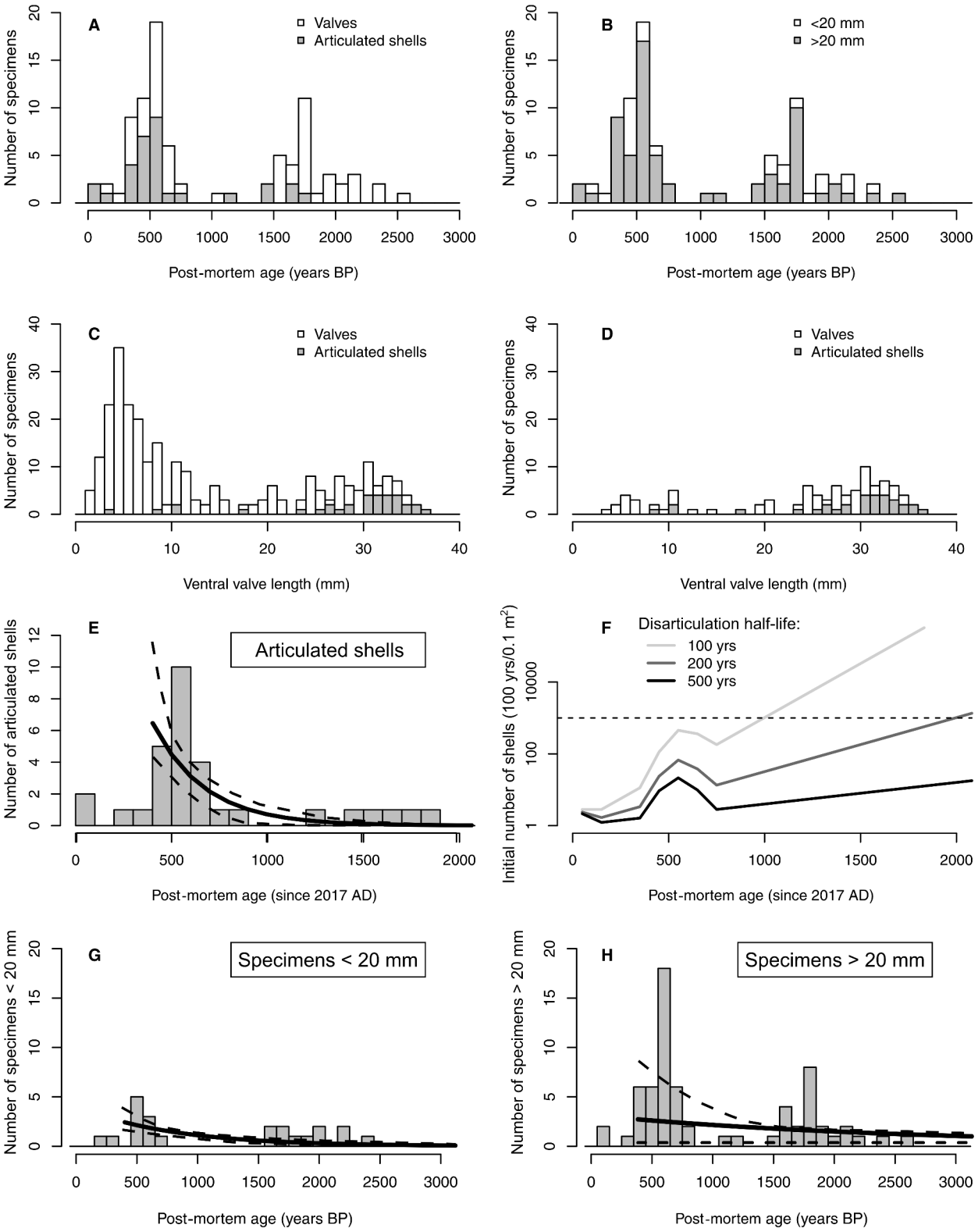

of the three oldest specimens fall between 18 210 and 25 620 years, and the age of one specimen is 7360 years. All of the other 88 specimens are younger than 3000 years. Time averaging (inter-quartile age range, IQR) of all *G. vitreus* specimens is 1250 years. The oldest articulated shell is 1770 years old, and the IQR of articulated shells is 200 years. In contrast to the bimodal age distribution of all specimens, distribution of post-mortem ages of articulated shells possesses just one mode, equivalent to the first mode at 500 years BP (Fig. 2E). The size-frequency distribution is also bimodal, with abundant small-sized, mainly juvenile specimens smaller than 10 mm, and with a second mode formed by shells 25–30 mm long (Fig. 2B, C). Although ventral valves (n = 160) are more frequent than dorsal valves (n = 92) in the total assemblage, no significant bias in the ratio of ventral and dorsal valves occurs in specimens exceeding 5 mm (96 ventral vs 70 dorsal valves, respectively).

Disintegration and disarticulation rate

The fitting of the simple model (that assumes that *G. vitreus* abruptly declined in abundance to zero at 450 years BP and that disintegration rate does not decline with post-mortem age) to post-mortem age data shows that disintegration rate of small individuals (<20 mm) is $\lambda_d = 0.0013$ year^{-1} (half-life is *c.* 530 years, Fig. 2G) and disintegration rate of larger individuals (>20 mm) is $\lambda_d = 0.00041$ year^{-1} (half-life is *c.* 1700 years, Fig. 2H). Fitting the same model to ages of articulated shells, assuming a simple age-independent disarticulation, indicates that disarticulation rate λ_a is 0.0036 year^{-1} (95% CI = 0.0023–0.0082; Fig. 2E). Disarticulation half-life is, therefore, surprisingly long (*c.* 200 years). Shorter half-lives are less likely because they predict unrealistically high population densities, exceeding 1000 individuals/m^2 (Fig. 2F), whereas the maximum density of *G. vitreus* recorded in the Mediterranean Sea is 700 individuals/m^2 (Emig 1987, Emig & García-Carrascosa 1991). For example, the 100-year age cohort with midpoint at 1550 years BP is represented by one articulated shell in the DA. Dividing the number of preserved shells by $e^{-\lambda a \times 1550}$, and if disarticulation half-life is equal to just 100 years, the model predicts that *c.* 46 000 shells entered the sediment over 100 years (at the scale of Van Veen grab, 0.1 m^2). This estimate propagates to an unrealistic annual density of *c.* 4600 individuals/m^2 (assuming that lifespan is *c.* 10 years; Tomašových *et al.* 2022*a*). In contrast, if disarticulation half-life is 200 years, the model predicts that 300 shells entered the sediment over 100 years, with a more realistic average annual density of *c.* 30 individuals/m^2 (Fig. 2F).

Brachiopod preservation

Encrusters on both internal and external valve surfaces are represented by serpulids, agglutinated polychaetes, bryozoans, and calcareous and agglutinated foraminifers, with preservation varying from complete specimens to eroded relicts (Fig. 3C, D). The etched scars were produced by anomiid bivalves (*Centrichnus eccentricus*; e.g. Neumann *et al.* 2014) (Fig. 3A, B). *Podichnus* traces, which represent brachiopod pedicle attachment scars (Bromley & Surlyk 1973), were not detected. Abundant dendritic or rosette-like traces (*c.* 0.25–0.5 mm in diameter) occur immediately below the external primary layer of most specimens (Fig. 3D–L). These subsurface traces are visible as whitish discrete dots on external surfaces in reflected light and as dark spots in transmitted light (Fig. 4A–D). They are formed by inter-connected oval chambers arranged in spirals (Fig. 3H, I) that are connected to the surface by thin filaments immediately below the primary layer (Fig. 4E–G). The chambers can be directly exposed on the surface as small pits or depressions when the primary layer is eroded (Fig. 3G). They can be assigned to the ichnogenus *Nododendrina* that was probably produced by endolithic foraminifers. This ichnogenus and similar dendritic and rosetta-producing borers have been characteristically infesting valves of punctate brachiopods since the Palaeozoic (Bromley *et al.* 2007; Wisshak 2017; Mergl 2020).

Macroborings formed by clionaid sponges (ichnogenus *Entobia*) are frequent on *G. vitreus*, producing oval chambers connected by thin ducts, clearly visible in transmitted light (Fig. 4A, B). In specimens where papillar openings occur on both valve surfaces, external surfaces are pitted with openings more frequently than internal ones. These papillar openings on internal surfaces can terminate with black or rusty Mn or Fe-rich sediments (Fig. 4H, I, K–M). With the exception of two specimens (out of 30 shells), which show calluses that partly (Fig. 4H, I) or completely (Fig. 4J) plug these openings, they remain open on internal surfaces. *Entobia* is extensive in the umbonal region of a few specimens where it is responsible for the exposure of the umbonal cavity.

Regardless of valve preservation, external and internal surfaces do not show any signs of fibre jagging or delamination of the whole secondary layer, made up of fibres. Fibre jagging or delamination is typical of the softening observed on brachiopod valves elsewhere in shallow-marine environments (Emig 1990; Tomašových & Rothfus 2005). Although we did not observe this type of preservation on *G. vitreus* specimens, the lack of peripheral margins in fragments and their sharp termination that exposes the anterior margin of the prismatic layer indicates that the softening and loss of the secondary

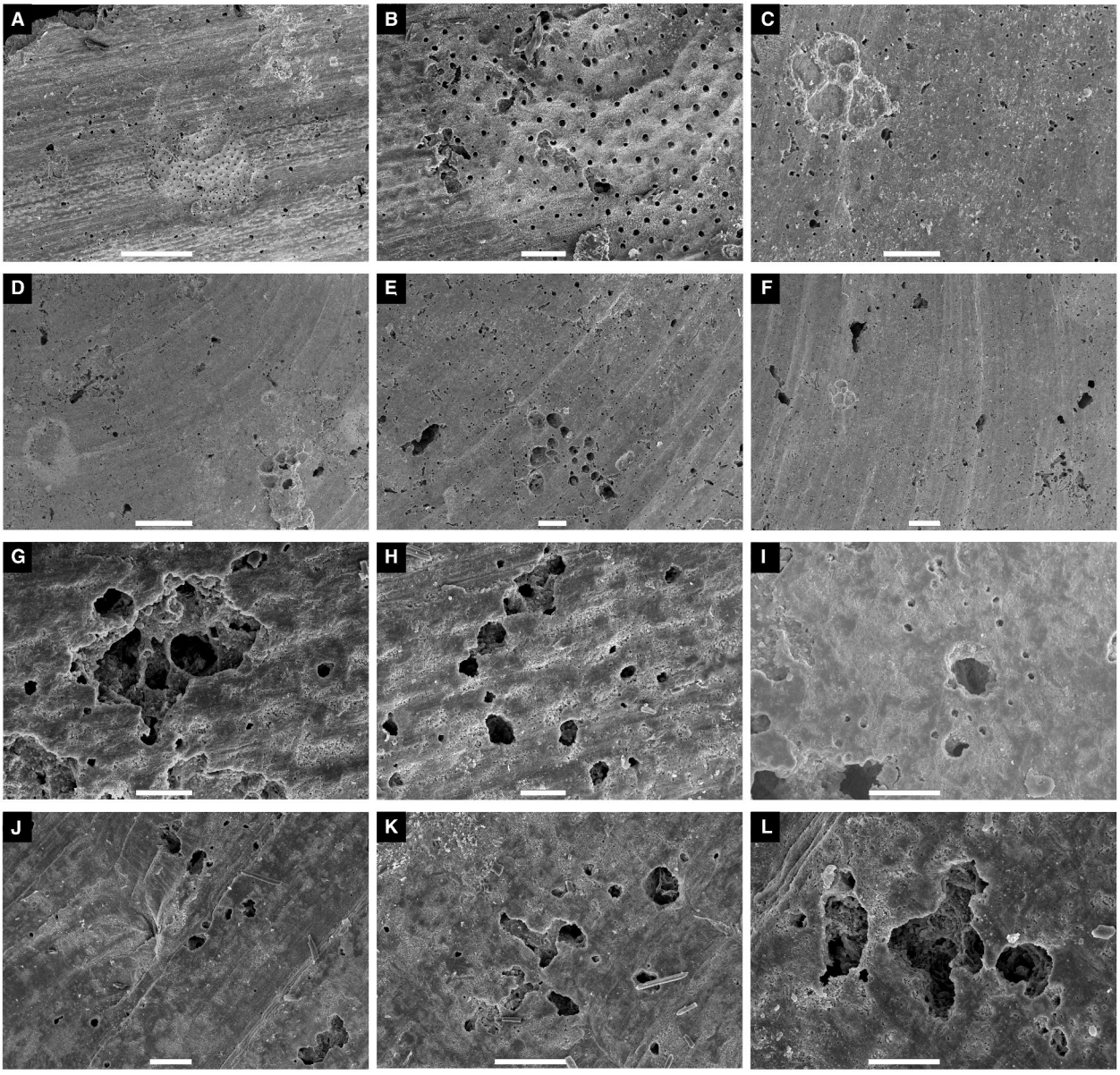

FIG. 3. Scanning electron micrographs of external surfaces of *G. vitreus* valves with scars produced by encrusters and microendolithic traces. A–B, an etched scar caused by the anomiid bivalve (ichnogenus *Centrichnus*). C, an eroded relict of an encrusting foraminifera. D, external surface with fragments of agglutinated foraminifers and microborings (*Nododendrina*); specimen 111. E–L, valves penetrated by endolithic foraminifers that are located immediately below the surface and are connected with the surface with thin filaments (ichnogenus *Nododendrina*): E–F, specimen 111; G–H, specimen 43–11; I, specimen 193; J–L, specimen 15. Scale bars represent: 500 μm (A, D), 100 μm (B, C, E, J, K), 200 μm (F), 50 μm (G–I, L).

layer along the anteriormost edges contributed to disintegration of the valves (Fig. 4M).

Fibres of the secondary layer and prisms of the tertiary layer on internal surfaces (penetrated by punctae, 5–10 μm in diameter) of *G. vitreus* are either smooth in pristine valves not affected by abrasion or discolouration (Fig. 5A–E), or affected by extensive networks of microborings (10–20 μm in diameter, Fig. 5G, H). They can be covered by <1 μm-size angular-shaped calcitic overgrowths and coccoliths (Fig. 5F). In contrast, internal surfaces of prisms and fibres of discoloured and worn valves are irregular, covered by thin micrometric patches of micrite crystals and by clay–coccolith coatings that occur in depressions at prism or fibre boundaries (Fig. 5J–L). In contrast to the low-Mg calcite that forms brachiopod valves (Fig. 6A), micrite cements that co-occur with clay coatings are formed by calcite enriched in Mg (Fig. 6A–C). Micrite cements and clay coatings are limited to valve surfaces, to internal

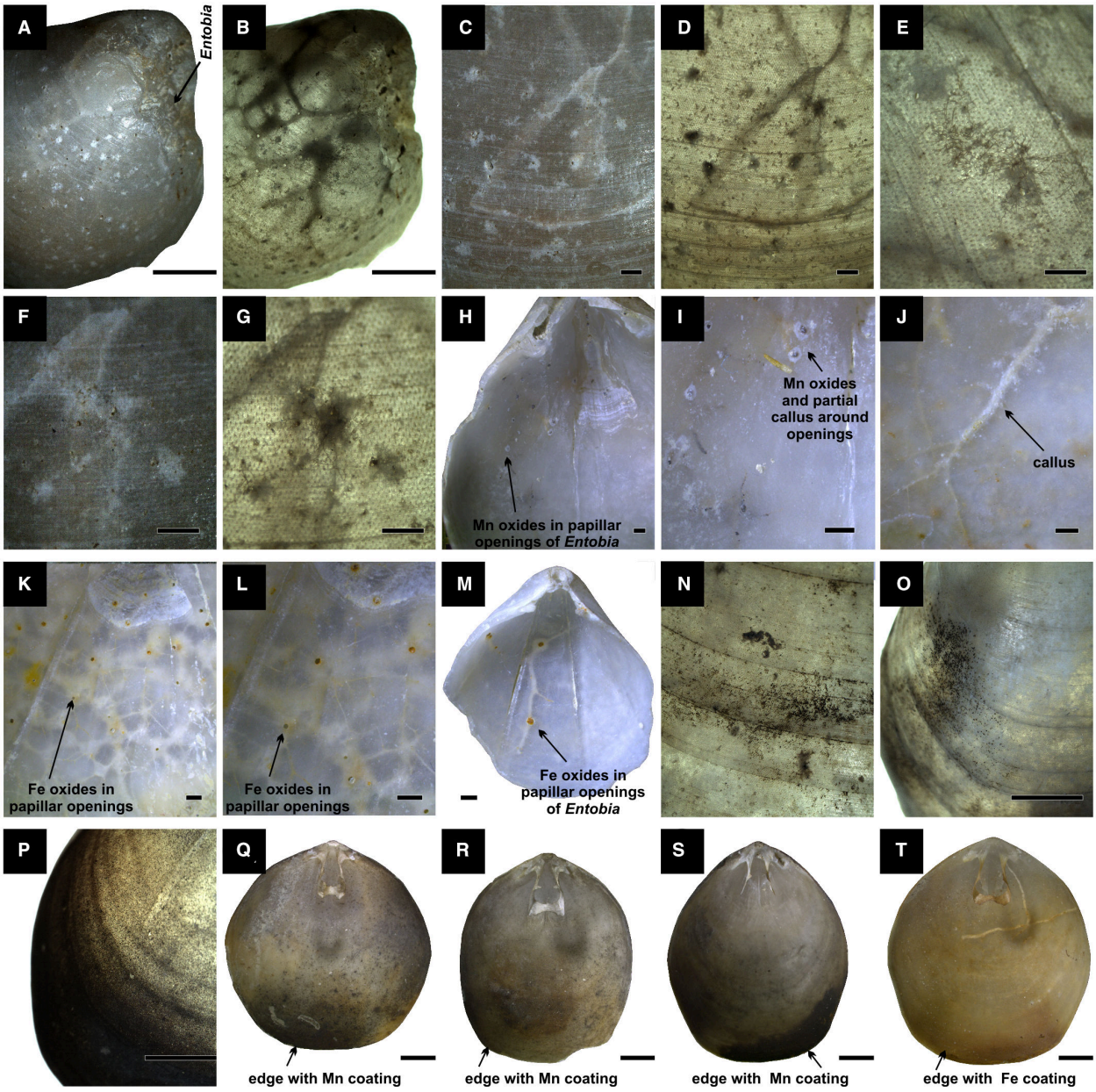

FIG. 4. Preservation of rosetted trace fossils (A–G) and *Entobia* (A–B, H–M) under reflected and transmitted light, and ferromanganese coatings and fillings of borings and punctae on the external (N–P) and internal surfaces (Q–T). A–B, dispersed rosetted microborings and internal galleries formed by *Entobia* in reflected (A) and transmitted (B) light; these galleries lead to the detachment of a large umbonal area in the posterior part of the ventral valve (arrow); specimen 43–1. C–G, rosetted and dendritic microborings (*Nododendrina*) on the external surface in reflected and transmitted light; specimen 43-11. H–I, internal valve surfaces with papillar openings of clionaid sponges and their diagenetic infill, with partial callus around openings, which are plugged with black aggregates formed by Mn oxides; specimen 42-2. J, exposed borings of clionaid sponges on the internal surface, healed with callus (specimen 3). K–M, papillar openings of *Entobia* on the internal surface without any callus and plugged with rusty Fe oxides: K–L, specimen 3; M, specimen 203. N–O, microborings and punctae on the external surface filled with black Mn oxides; specimen 25-1. P, black coating formed by Mn oxides viewed from the exterior in transmitted light; specimen 7. Q–T, interior of valves with Mn-coated edges (Q–S) and Fe-coated edges (T): Q, specimen 2; R, specimen 5; S, specimen 8; T, specimen 23. Scale bars represent: 5 mm (A, B, O–T); 1 mm (C–N).

punctal infills, and borings. Freshly-broken valve edges in the same specimens, however, show that fibres or prisms within valves are smooth and well-preserved (Fig. 5I).

Black Mn oxides (Fig. 4Q–S) and rusty (reddish and orange) Fe oxides (Fig. 4T), validated by EDS spectra (Fig. 6D), are represented by aggregates of grains in mm-

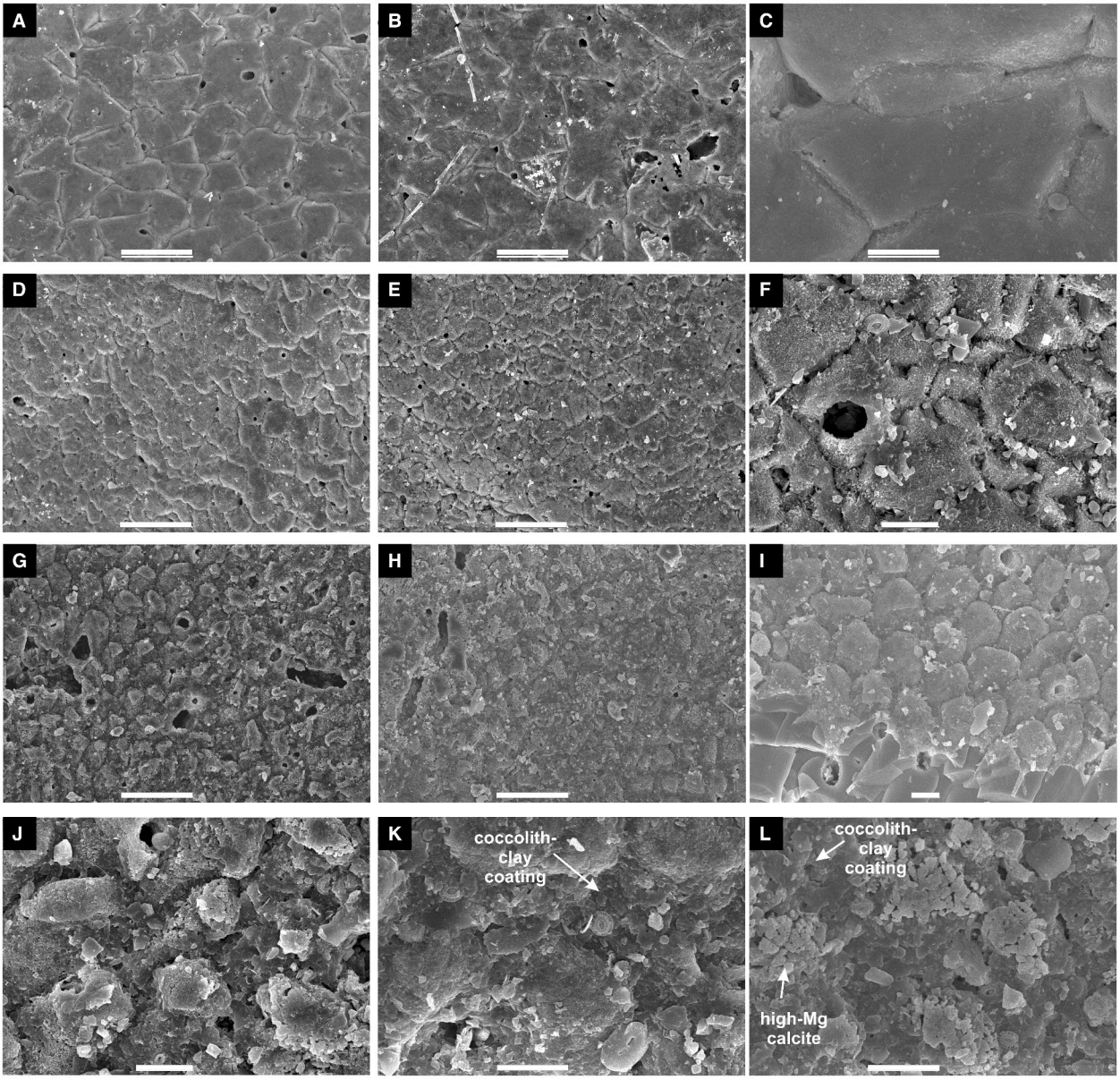

FIG. 5. Scanning electron micrographs showing the preservation of internal surfaces of *G. vitreus*, with two well-preserved valves (A–F) and one discoloured valve with microborings, clay coatings and micrite cements (G–L). A–C, well-preserved surface formed by prisms of the tertiary layer on the ventral valve, with smooth prism surfaces and dispersed punctae; specimen 191; C, close-up showing that the prism surface is smooth and lacking cement. D–F, a relatively well-preserved internal surface of the dorsal valve, with the transition from secondary fibres to prisms close to the hinge (D) and with prisms (E); specimen 143; F, close-up showing that surface of prisms is overgrown by micron-sized calcitic crystals and covered by coccoliths. G–L, microborings, clay–coccolith coatings among prisms, and micrite cements on the surfaces of prisms; specimen 194; the clay coatings and cements occur on surfaces or within borings, whereas freshly-broken edges are pristine (I). Scale bars represent: 50 μm (A, B, D, E, G, H); 10 μm (C, F, I–L).

scale spots, or form continuous coatings (*c.* 0.1 mm thick) that are sharply separated from the valve surface (Fig. 7). The coatings are particularly extensively developed on the internal surfaces of articulated shells along the anterior edges of both valves, whereas in central parts of valves they form dispersed, mm-scale spots (Fig. 4Q–T). They fill punctae and borings, and plug the papillar openings of boring sponges on the interior surfaces of valves. Reddish and orange coatings are replaced by black coatings across few millimetres on the internal surfaces of some valves, and both smooth globules (Mn oxides) and tufts (Fe oxides) co-occur in transition zones (Fig. 7E–H). At high magnification (>500×), Fe oxides are represented by tufts (10–20 μm in diameter)

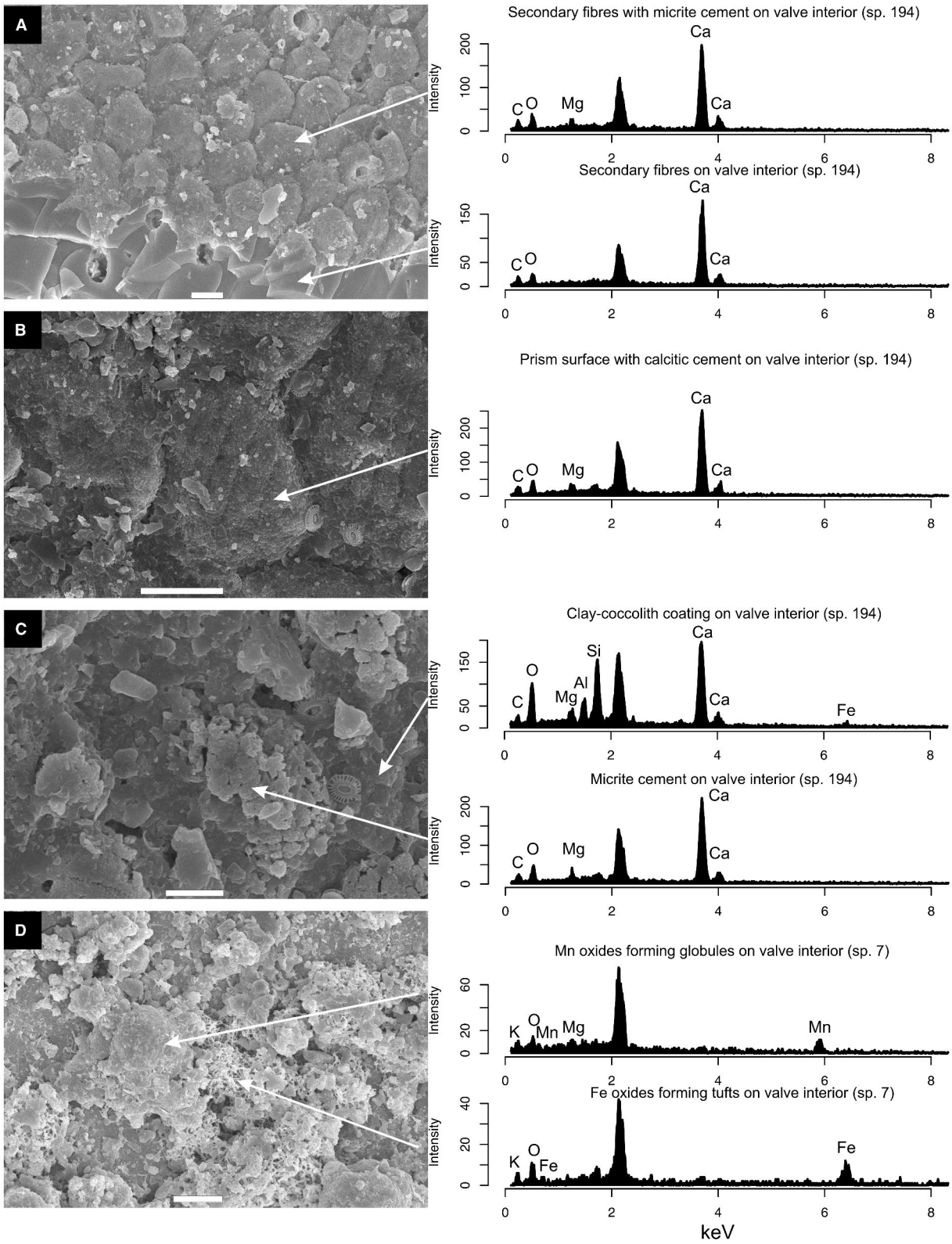

FIG. 6. Scanning electron micrographs and corresponding EDS spectra. A, low-Mg calcite of pristine valves. B, calcite overgrowths enriched in Mg in thin micritic cements. C, clay coatings and micritic cements. D, Mn and Fe oxides represented by globules and tufts, respectively. The peak in at 2.2 keV corresponds to the gold coating. Scale bars represent: 10 μm (A, B, D), 5 μm (C).

and Mn oxides by smooth globules (10–50 μm in diameter). These tufts or globules are either dispersed, or coalesce to continuous coatings (Figs 6D, 7). The Mn globules are similar to stalactitic Mn-rich aggregates coating serpulid tests in the Jabuka Pit in the Central Adriatic Sea (Dolenec 2003).

Variation in preservation among specimens

With the exception of eight specimens, other articulated shells of *G. vitreus* (n = 24) were completely filled with sediment (Fig. 8). Brachidia were fully preserved in 53% of articulated shells, whereas they were broken or fully missing in all of the disarticulated dorsal valves (Fig. 9). *Gryphus vitreus* is preserved in three states, including: (1) articulated, sediment-filled shells with complete lophophore supports, rare or absent internal encrusters and borers, and internal ferromanganese coatings (post-mortem age up to 1800 years) as documented by EDS spectra (Fig. 6); (2) complete or almost complete, semi-transparent or white disarticulated valves of similar age but frequently with both internal and external encrusters and borers (age up to 2300 years; Fig. 10A, B); and (3) umbonal relicts that are worn, discoloured (covered with micrometric clay and micritic coatings, Fig. 10C–L), with missing anteriormost edges (that were formed by the secondary fibrous layer), with truncated valve relicts formed largely by the prismatic layer only (Fig. 10C–E). This third category also includes few specimens from the last glacial maximum (age > 18 000 years; Fig. 10C–L).

These preservational states are also exhibited by smaller, juvenile valves (<10 mm), ranging from well-preserved and transparent valves without any alteration, to fragments that are intensely microbored, discoloured and stained (Fig. 11). Brownish discolouration is primarily associated with the presence of clay coatings and micrite cements that are locally also associated with patches of Fe oxides; we did not observe pyrite grains in discoloured valves (Kolbe *et al.* 2011).

In the total assemblage, 80% of individuals are disarticulated, 75% are fragmented and 17% discoloured (Fig. 12A). If specimens are not partitioned into shells and disarticulated valves, encrustation frequencies are

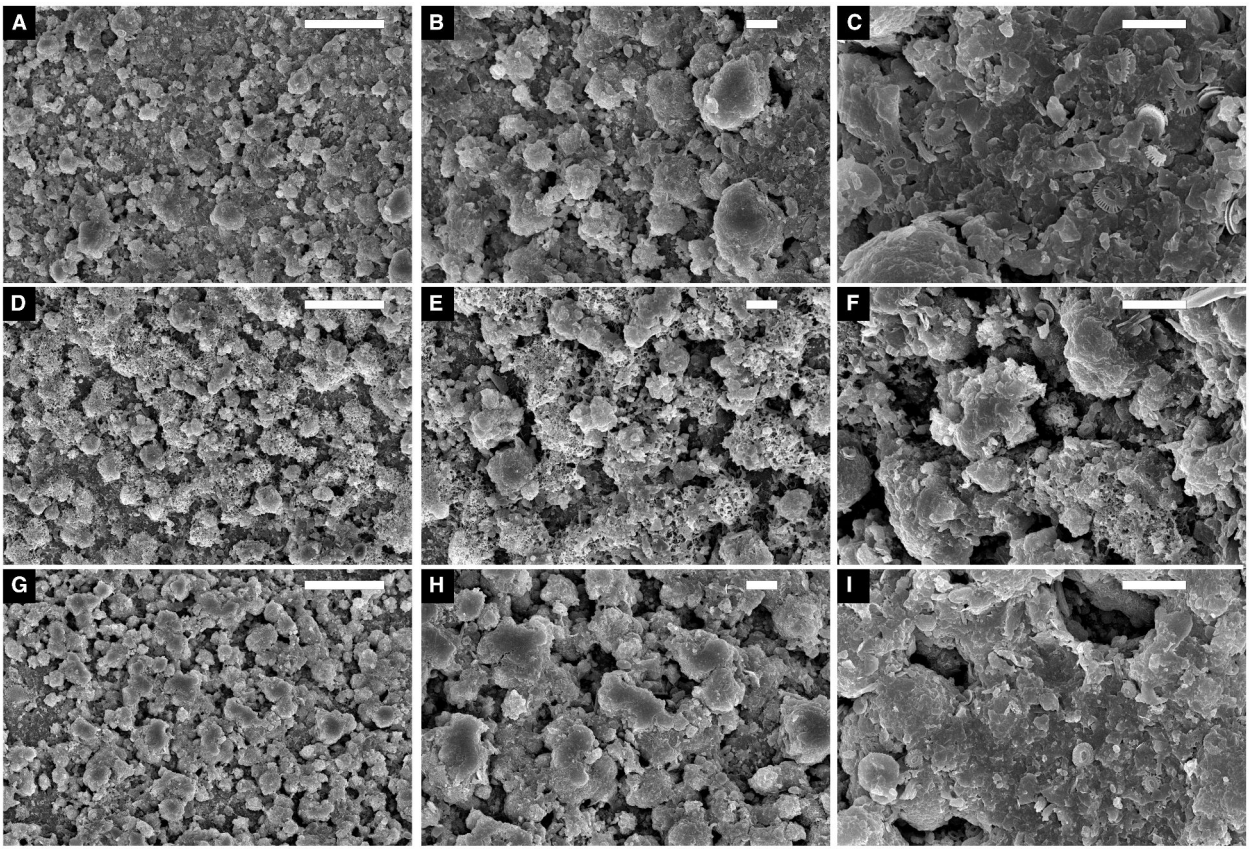

FIG. 7. Scanning electron micrographs of internal surface of brachiopod valves with Fe-oxide tufts and Mn-oxide globules on specimen 7 (445 years BP). A–D, smooth Mn-oxide globules that are dispersed or loosely-packed. E–H, the mixture of Mn-oxide globules and Fe-oxide tufts. I–L, a continuous coating formed by densely-packed Mn-oxide globules. Scale bars represent: 50 μm (A, D, G), 10 μm (B, C, E, F, H, I).

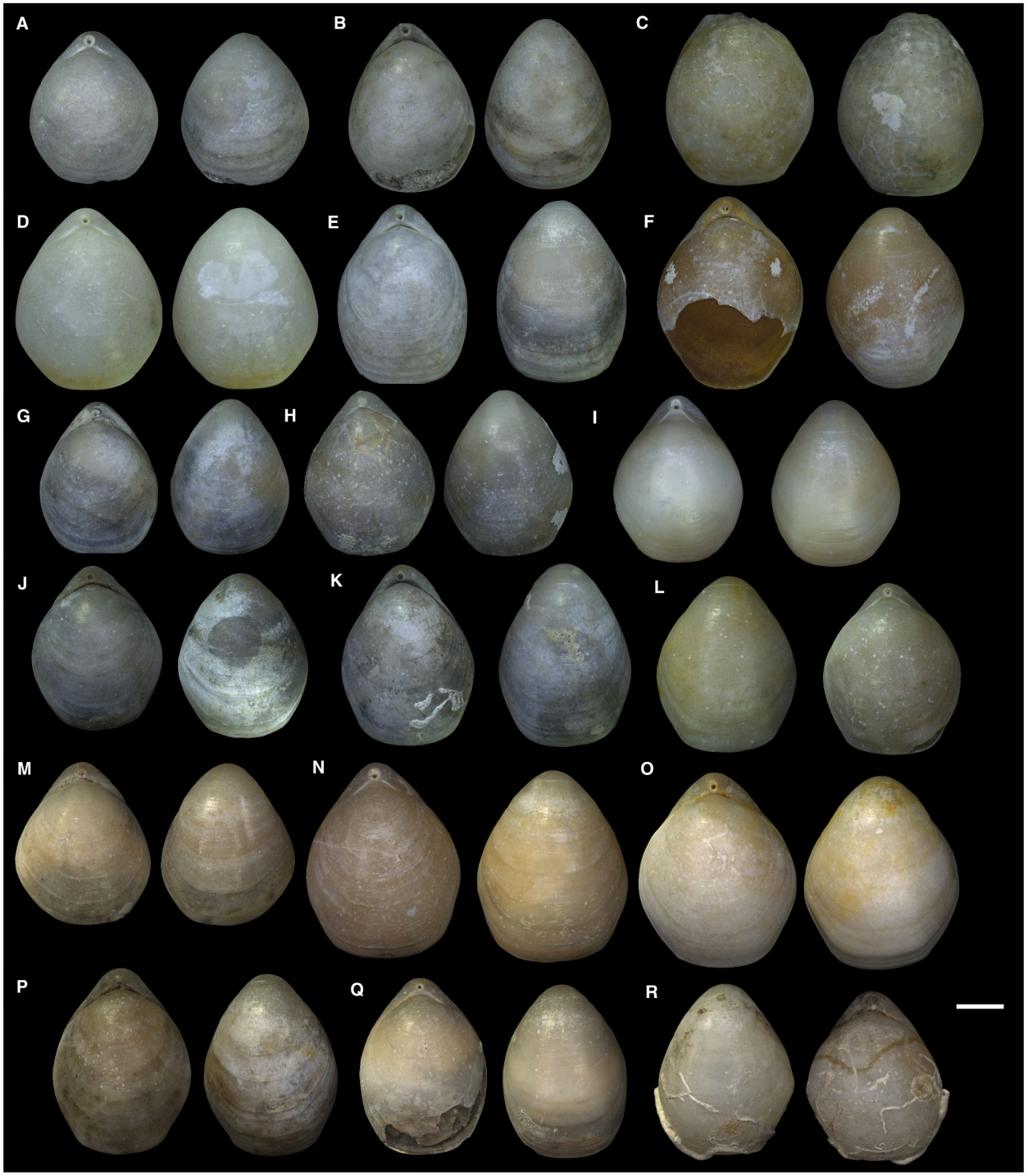

FIG. 8. Articulated shells of *G. vitreus* ranging in age from several centuries up to *c.* 1800 years. The specimens in D, E, F, I and N were empty, other specimens were completely filled with sediment when photographed. The dark-grey and rusty colours reflect precipitation of Fe and Mn oxides on internal surfaces. Specimen numbers (post-mortem age): A, 13 (584 years); B, 10 (429 years); C, 3 (1418 years); D, 1 (not dated); E, 5 (552 years); F, 6 (1771 years); G, 7 (191 years); H, 12 (497 years); I, 15 (529 years); J, 14 (481 years); K, 8 (386 years); L, 17 (1655 years); M, 22 (304 years); N, 23 (398 years); O, 24 (1500 years); P, 25 (668 years); Q, 34 (505 years); R, 37 (postbomb). Scale bar represents 10 mm.

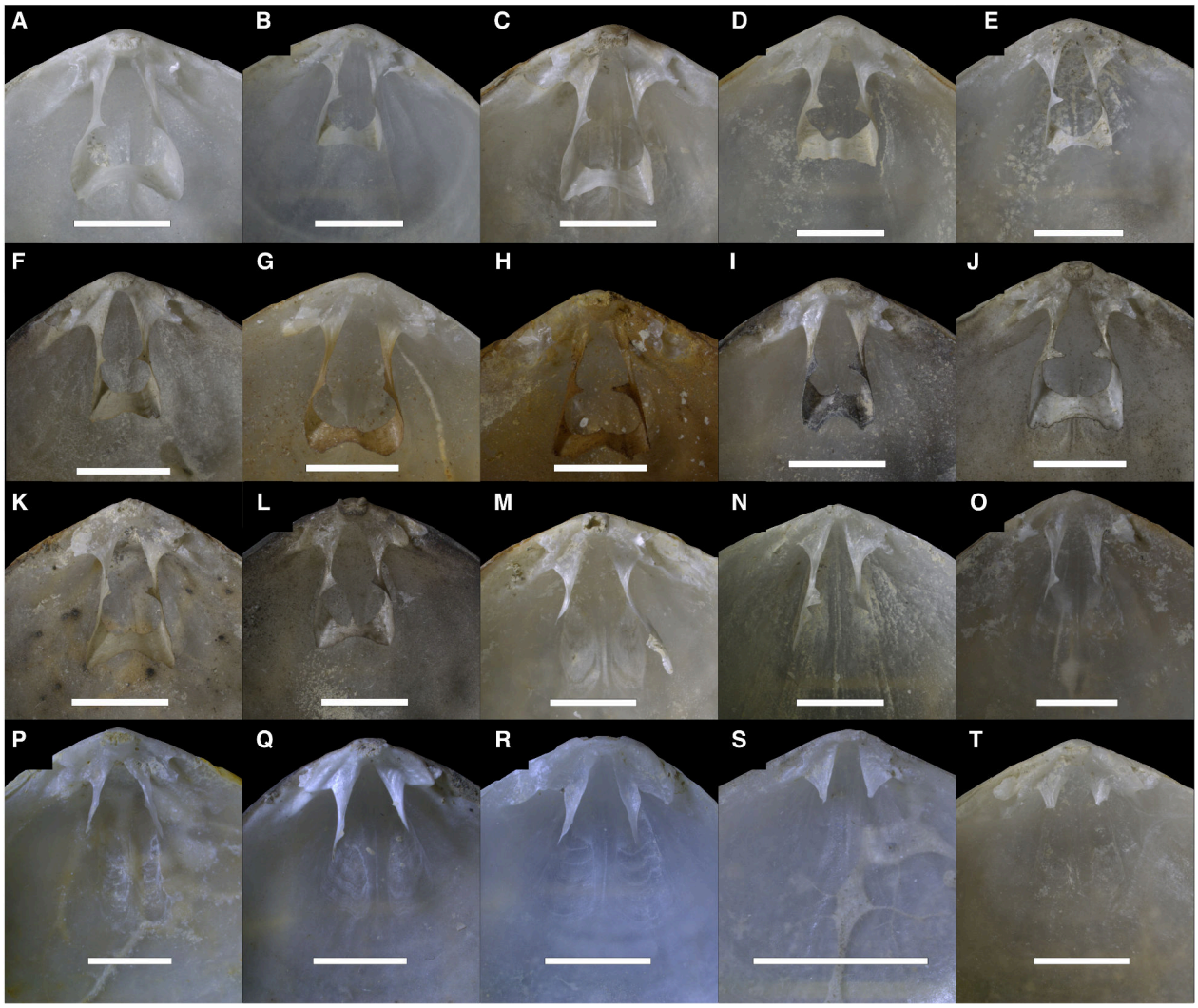

FIG. 9. Preservation of complete loops (A–O) and hinge plates with broken or missing loops (P–Y) in several centuries old but still articulated shells. A–F, complete loops without any Mn or Fe oxides; specimens (post-mortem age): A, 1 (not dated); B, 39 (758 years); C, 37 (postbomb); D, 15 (529 years); E, 13 (584 years); F, 22 (304 years). G–H, complete loops coated by rusty Fe oxides: G, 23 (398 years); H, 6 (1771 years). I–L, complete loops coated by black Mn oxides: I, 7 (191 years); J, 5 (552 years); K, 12 (497 years); L, 14 (481 years). M–Q, incomplete loops with descending lamellae: M, 24 (1500 years); N, 30 (postbomb); O, 34 (505 years); P, 3 (1418 years); Q, 10 (429 years). R–T, hinge plates only: R, 11 (521 years); S, 57 (427 years); T, 17 (1655 years). All scale bars represent 5 mm.

equally high on external (27%) and internal surfaces (28%) respectively. In contrast, boring frequencies are higher on external (20% by sponges and 79% by microborers) than on internal valve surfaces (11% by sponges and 50% by microborers). The frequencies of abrasion are similarly high on external (19%) and on internal surfaces (14%), as are the frequencies of valve exteriors and interiors coated by Fe oxides (11–15%) and Mn oxides (7–10%). PCoA based on all alteration indices and on all the specimens shows that most variables positively covary with the principal co-ordinates axis (PCo) 1 (74% of variance explained), whereas PCo2 explains only 14% of the variance (Fig. 13A). In contrast to all of the other variables, the coatings of Fe and Mn oxides, and disarticulation correlate weakly with PCo1 ($r < 0.5$), and are strongly correlated with PCo2, together with external encrustation and macrobioerosion ($r > 0.5$). PCo2 thus separates articulated shells with Fe and Mn oxides on internal surfaces from disarticulated, more altered valves (Fig. 13A).

Differences in preservation between articulated shells and disarticulated valves

The extent of external encrustation, as well as micro- and macrobioerosion is similar on external surfaces of

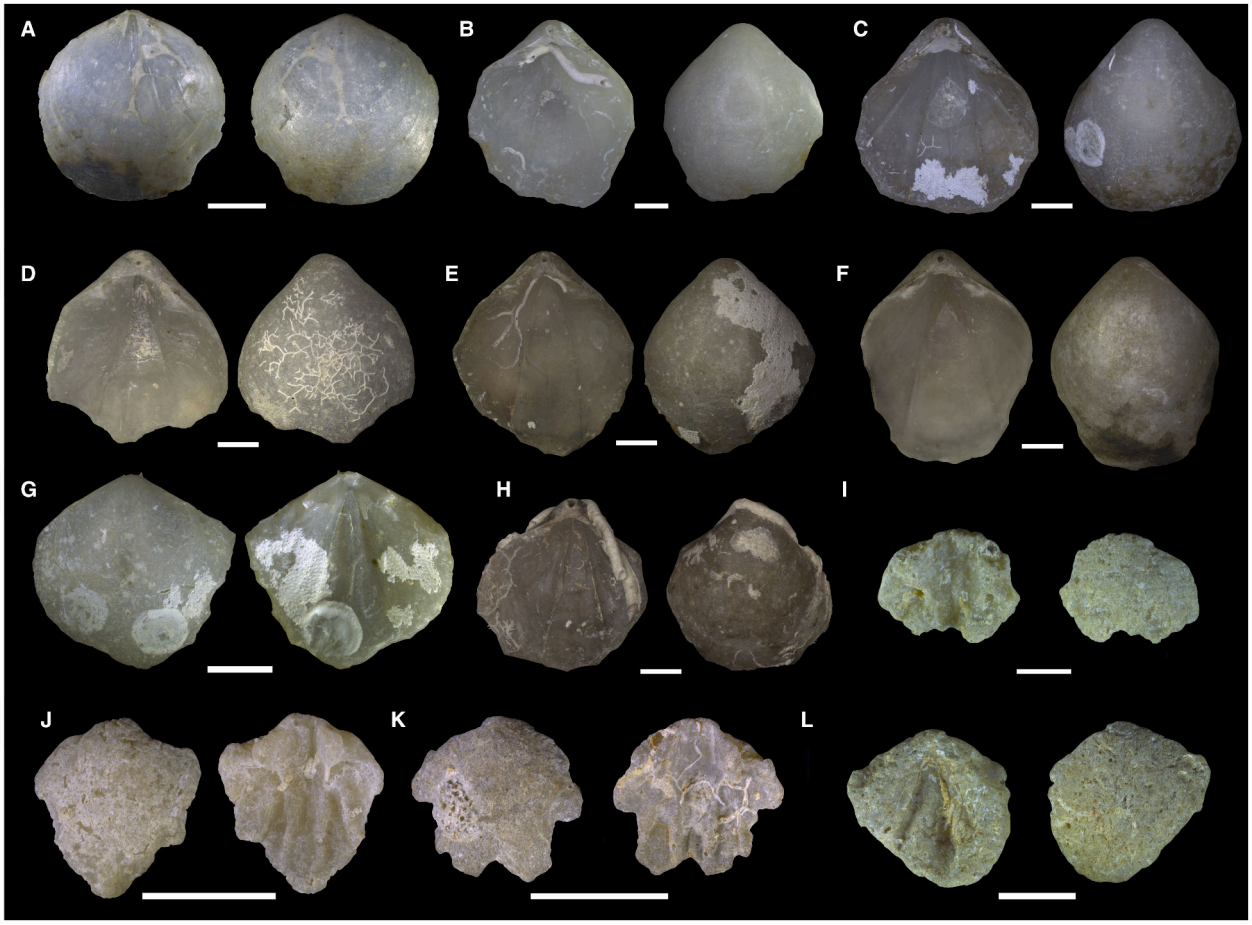

FIG. 10. Variability in preservation of disarticulated valves, with umbonal relicts older than 18 000 years. A, well-preserved dorsal valve with *Entobia* and black Mn-oxides close to the anterior edge (specimen 57; 427 years). B, fragment of ventral valve with missing peripheral margins and serpulids encrusting internal surface (specimen 38-1; 1633 years). C, ventral valve with missing anterior edge, encrusted on both valve surfaces, with patches of black and brownish coatings on the exterior along the anterior edge (specimen 42-1; 357 years). D, ventral valve relict affected by discolouration, encrusted by agglutinated foraminifers on the exterior, with anterior margin missing (specimen 41-2; 378 years). E, brownish ventral valve fragment, encrusted on the interior and exterior (specimen 43-3; 537 years). F, dorsal valve with chipped edges, with a black coating near the external anterior margin (specimen 43-5; 581 years). G, rounded fragment of dorsal valve encrusted on both surfaces (specimen 46; 1054 years). H, brownish ventral valve fragment, encrusted on both surfaces with well-preserved bryozoans and serpulids (specimen 27; 493 years). I, discoloured ventral valve fragment with worn encrusting foraminifers (specimen 45; 18 213 years). J, worn umbonal relict of ventral valve (specimen 67; 24 881 years). K, worn and discoloured umbonal relict of dorsal valve, with well-preserved foraminifers encrusting truncated internal surfaces (specimen 64; 7364 years). L, worn and discoloured dorsal valve relict with eroded encrusters (specimen 44; 2574 years). All scale bars represent 5 mm.

articulated shells and disarticulated valves. Interiors of disarticulated valves, however, are more strongly encrusted and bored than the interiors of articulated shells. These articulated shells display moderately-high levels of external encrustation (PSA = 0.18), macrobioerosion (PSA = 0.24), and microbioerosion (PSA = 0.57) but only minor levels of internal encrustation, macrobioerosion and microbioerosion (all PSA < 0.1; Fig. 12B). External and internal surfaces of disarticulated valves show similarly high levels of encrustation (PSA = 0.19 (ext.), 0.2(int.)), macrobioerosion (0.13, 0.07), and microbioerosion (0.63, 0.41). Therefore, although external surfaces of whole shells and disarticulated valves are affected by encrustation and bioerosion to a similar extent, internal surfaces are more encrusted and bored in disarticulated valves than in whole shells. Fe and Mn oxides are more frequent on internal valve surfaces within shells (PSA (Fe oxides) = 0.21, PSA (Mn oxides) = 0.45) than on their external surfaces (PSA (Fe oxides) = 0.08, PSA (Mn oxides) = 0.15). In contrast, both interiors and exteriors of disarticulated valves are coated equally frequently (PSA (Fe oxides) = 0.06, 0.08; PSA (Mn oxides) = 0.02 on both surfaces).

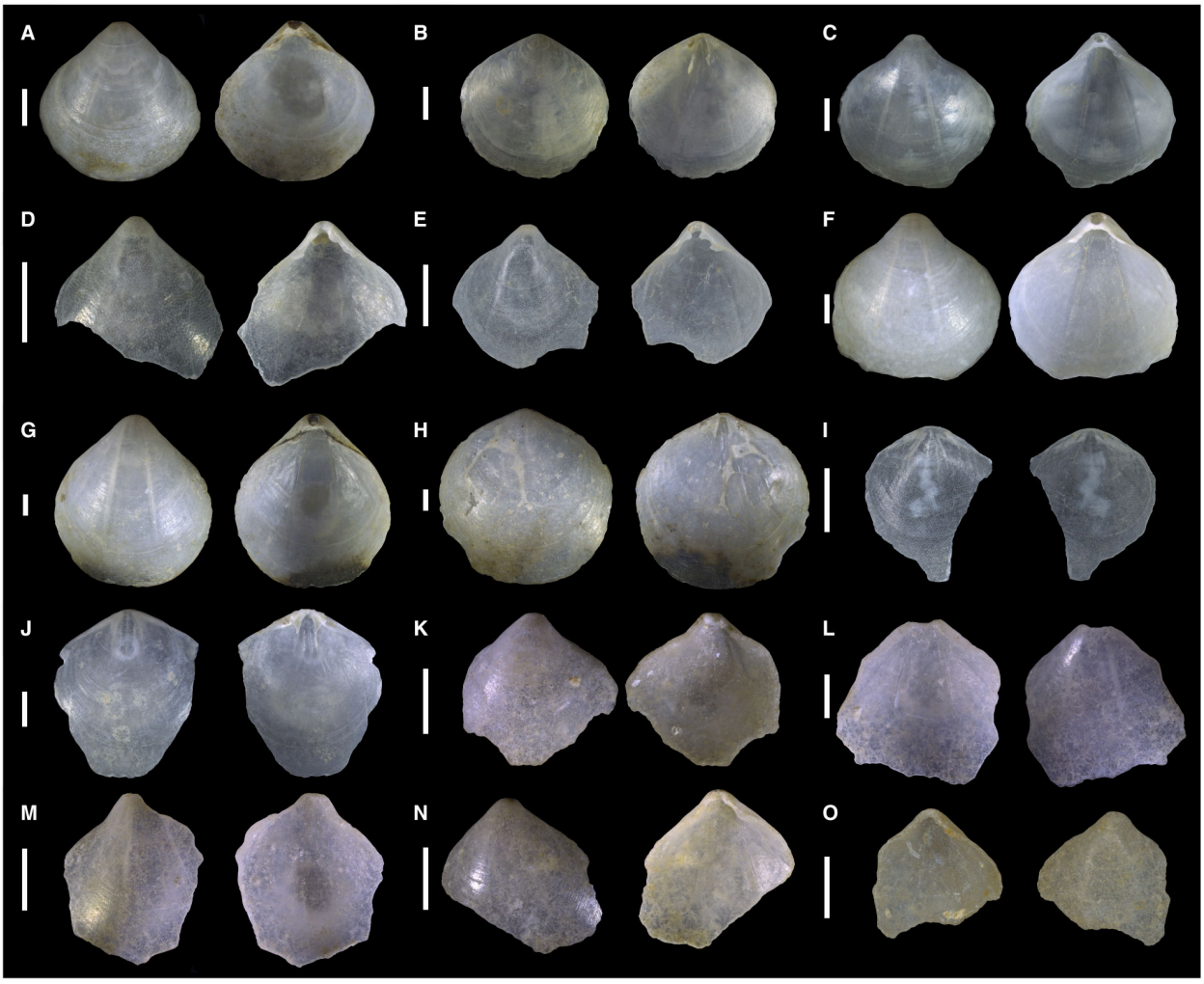

FIG. 11. Preservation of small-sized (juvenile) specimens ranging from well-preserved, semitransparent valves (A–F) to valves with internal coatings by Mn-oxides (G, H) to brownish-discoloured and microbored fragments with punctae stained by iron oxides (K–O). Specimen numbers (post-mortem age): A–B, complete shell, 55 (496 years); C, relatively complete ventral valve, 47 (1619 years); D, fragment of transparent ventral valve, 74 (1769 years); E, fragment of semitransparent ventral valve, 76 (1580 years); F, white ventral valve with a chipped anterior margin, 56 (412 years); G–H, complete shell with internal black coating near the anterior edge in both valves, 57 (427 years); I, fragment of transparent dorsal valve, 75 (1657 years); J, fragment of semitransparent dorsal valve, 58 (481 years); K, ventral valve fragment, with internal encrusters and common microborings stained by iron oxides, 62 (625 years); L, ventral valve fragment with internal encrusters and abundant microborings, 61 (1876 years); M, ventral valve fragment with microborings, 60 (2114 years); N, ventral valve fragment microborings stained by iron oxides, 72 (1974 years); O, brownish, discoloured fragment of ventral valve, 77 (522 years). All scale bars represent 2 mm.

Taphonomic clock

The proportion of articulated shells relative to the total number of individuals within 100-year cohorts exceeds 50% in age classes of 50, 450, 550, 1450 and 1650 years BP (Fig. 2A), thus reaching surprisingly high values even in specimens older than multiple centuries. Their contribution to the older cohorts declines and no specimens older than 1800 years are articulated (Fig. 2A). The post-mortem age correlates weakly with both PCoA axes (Spearman r: (PCo1) = 0.37, $p < 0.001$; (PCo2) = 0.22, $p = 0.036$). The effect of post-mortem age on alteration is also weak (CAP F (age) = 9.6, $p < 0.001$, R^2 = 17%, n = 92). When alteration is modelled as a function of both age and size, R^2 increases to 21% (CAP F (age) = 8.5, $p < 0.001$, n = 92). Although the explanatory power of these two variables is low, post-mortem age increases along the first CAP axis whereas small and large-sized specimens are separated along the CAP 2 axis (Fig. 13C). Articulated shells with negative CAP 1 scores are separated from disarticulated valves with positive CAP 1 scores, and specimens with the most positive

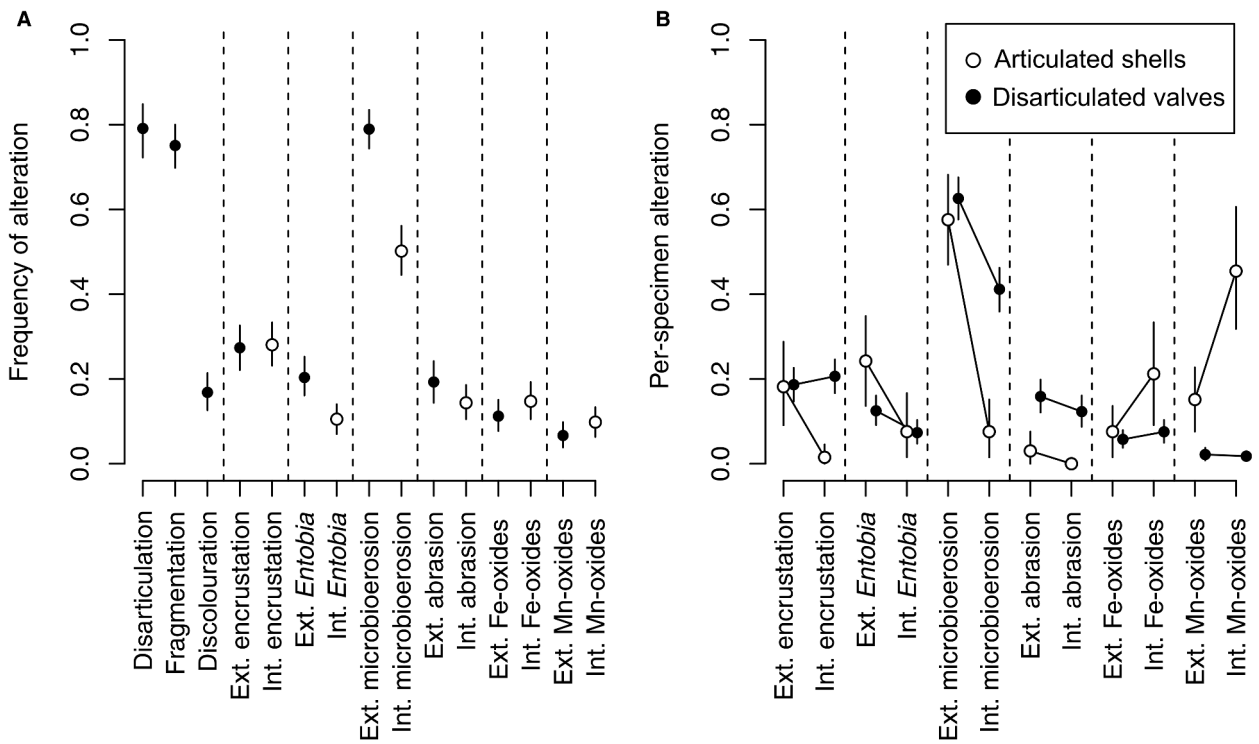

FIG. 12. A, frequency of alteration in all *G. vitreus* specimens, standardized to the number of individuals for disarticulation and to the total number of specimens for other variables, tends to be higher on external than on internal surfaces (with the exception of coatings by Fe and Mn oxides). B, per-specimen alteration (PSA) state partitioned according to disarticulation demonstrates that the difference in encrustation, micro- and macrobioerosion between external and internal surfaces is high in articulated shells, whereas it is low in disarticulated valves.

scores are represented by discoloured and abraded fragments. CAP thus visualizes two size-specific preservation pathways, with alteration progressing with increasing age along the CAP 1 axis (arrows in Fig. 13C).

The complexity of the taphonomic clock emerges in cohort-level analyses of specimens binned to eight cohorts (encompassing *c.* 20 000 years, Fig. 14). Specimens that are 100–1000 years old are rather similar but differ in alteration from specimens older than a few millennia. Age-dependency of alteration over the initial *c.* 2000 years is weak for most variables, with the exception of disarticulation and fragmentation (Fig. 14A). The four specimens older than 5000 years are not only represented by disarticulated fragments but are also heavily bioeroded, discoloured, encrusted and abraded. Across all age cohorts, post-mortem age positively correlates with the mean per-cohort disarticulation (Spearman r = 0.83, p = 0.011) and fragmentation (Spearman r = 0.9, p = 0.002), microbioerosion (Spearman r (exterior) = 0.83,

FIG. 13. A, principal co-ordinates analysis (PCoA) based on 15 variables shows the difference in overall preservation between articulated shells and disarticulated valves; contours correspond to ventral valve length (in mm) prior to fragmentation (extrapolated from fragments on the basis of reduced major axis regressions). B, the negative relation between the length of ventral valve and PCo2 demonstrates the size dependency of alteration; specimens with and without coatings formed by Fe and Mn oxides also possess negative scores along PCo2. C, constrained analysis of principal co-ordinates (CAP) maximizing the separation of specimens on the basis of shell size and post-mortem age, with contours representing post-mortem age, fitted to ordination scores with the generalized additive model the first axis correlates largely with post-mortem age and the second axis with shell size (ventral valve length prior to fragmentation); therefore, an increase in overall alteration with increasing post-mortem age along the CAP 1 axis, progressing from articulated shells to complete disarticulated valves and to disarticulated, discoloured and worn fragments, documents the direction of size-specific taphonomic pathways that generate the taphonomic clock; black circles and squares represent large shells and large disarticulated valves (>20 mm); white circles and squares represent small shells and small disarticulated valves (<20 mm); the size thresholds refer to the ventral valve length prior to fragmentation. Photographed specimens (with their numbers and post-mortem age): a, 22 (304 years); b, 24 (1500 years); c, 43.1 (537 years); d, 27 (493 years); e, 45 (18213 years); f, 58 (481 years); g, 76 (1580 years); h, 61 (1876 years); i, 46 (1054 years); j, 65 (2352 years).

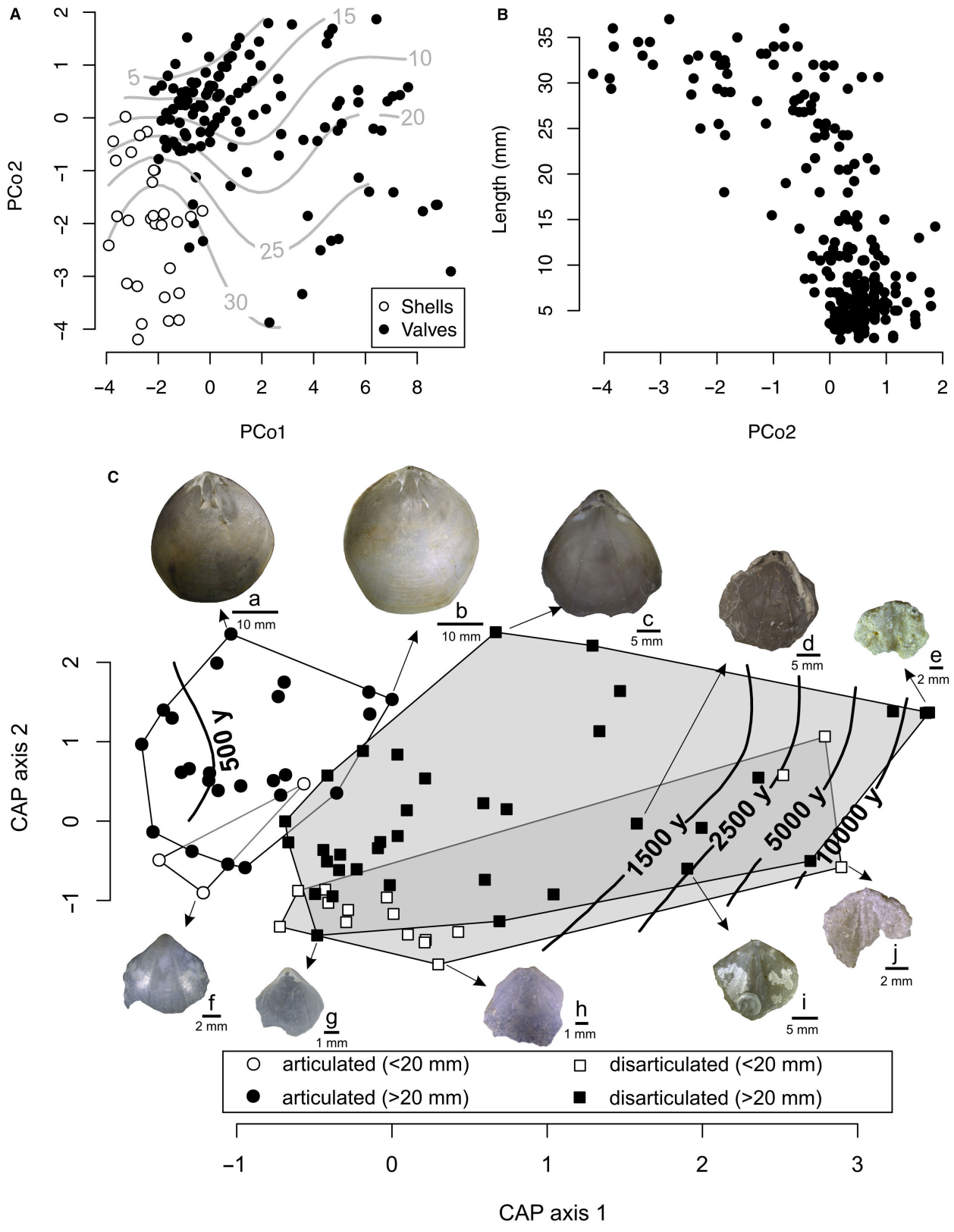

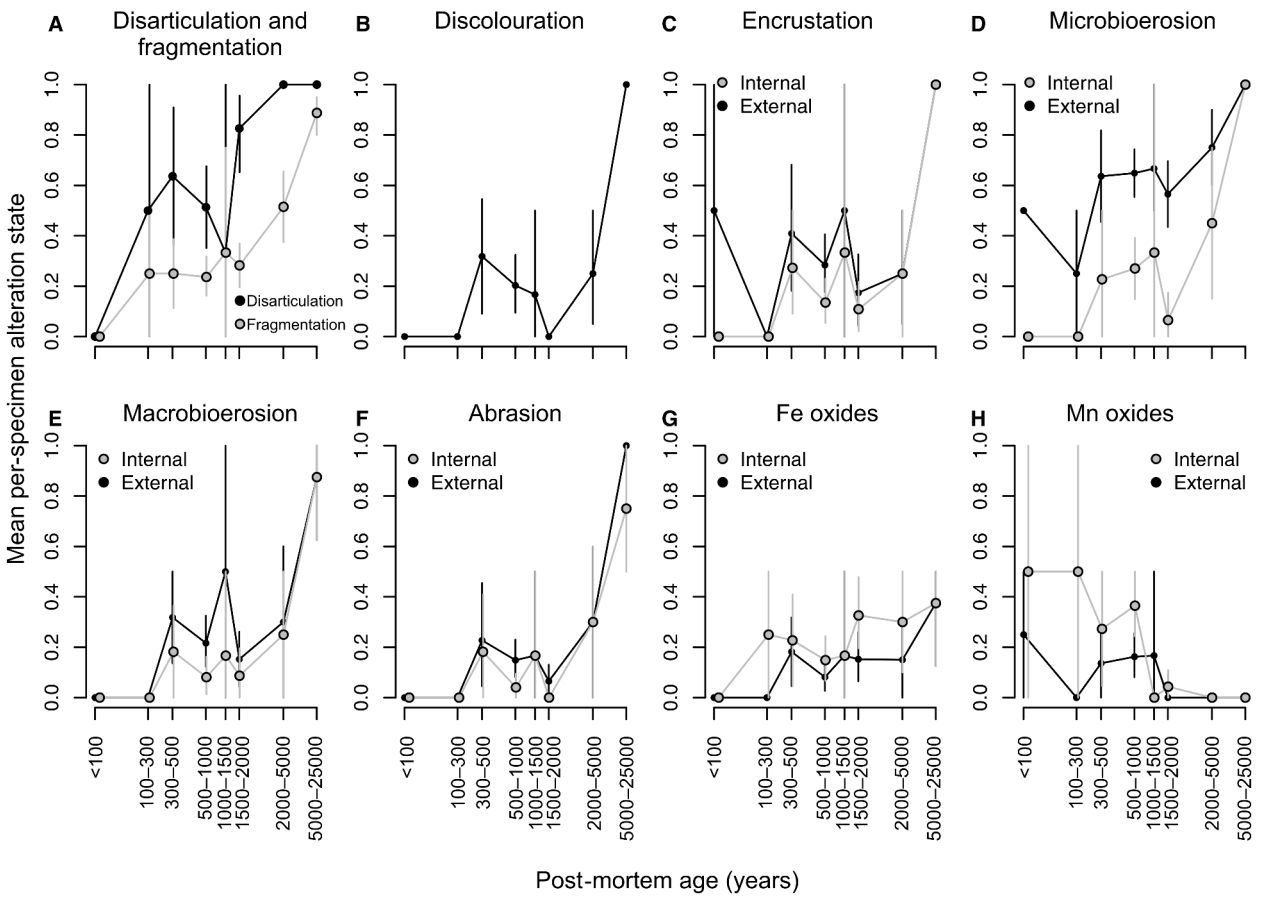

FIG. 14. Taphonomic clock on external (black) and internal surfaces (grey) of *G. vitreus*. A, disarticulation and fragmentation. B, discolouration. C, encrustation. D, microbioerosion. E, macrobioerosion. F, abrasion. G, Fe oxide coatings. H, Mn oxide coatings. Aggregating specimens into eight age cohorts (the oldest category includes four shells older than 5000 years) shows: (1) weak or no age dependency of alteration over the initial 2000 years (with the exception of disarticulation, fragmentation and coatings by Fe oxides; mean alteration by encrusters or borers does not increase with increasing age); and (2) age dependency of alteration becomes more apparent and significant over the whole range of post-mortem ages (>5000 years) because the four specimens older than 5000 years are strongly bored, encrusted and abraded. The mean extent of internal Mn oxides declines whereas the mean extent of internal Fe oxides increases with post-mortem age.

p = 0.015; r (interior) = 0.85, p = 0.007) and macrobioerosion (Spearman r (exterior) = 0.68, p = 0.06; r (interior) = 0.82, p = 0.011; Fig. 14). Post-mortem age also correlates moderately positively with discolouration, but high variability in the proportion of discoloured specimens in older cohorts (Fig. 14B) lead to inconclusive support for a discolouration-based clock (Spearman r = 0.56, p = 0.15). Interestingly, the mean per-cohort extent of Mn oxides on internal surfaces declines with post-mortem age (Spearman r = −0.89, p = 0.003, Fig. 14H) whereas the extent of Fe oxides on internal surfaces increases with post-mortem age (Spearman r = 0.76, p = 0.036, Fig. 14G).

Size dependency of preservation

PCo1 does not correlate with size (Spearman r = −0.03, p = 0.59) whereas PCo2 correlates negatively with size (Spearman r = 0.57, p < 0.0001, Fig. 13B). The direct ordination shows that at the scale of individual specimens, log-transformed size explains a minor amount (7%) of variation in alteration (F (size) = 13.92, p = 0.001, n = 257). However, aggregating specimens to 5 mm-bins shows that some types of alteration relate to size non-monotonically. First, the mean extents of internal encrustation, micro- and macrobioerosion, and discolouration increase up to a valve length of *c.* 20 mm, but decline to low values in specimens >20 mm (Fig. 15). Second, the mean per-cohort disarticulation monotonically declines with size (Spearman r = −0.93, p = 0.002) whereas the mean extent of internal Mn and Fe oxides increases with size (Spearman r = 0.93, p = 0.0007). Third, the mean extents of microbioerosion (Spearman r = 0.64, p = 0.09) and macrobioerosion (Spearman r = 0.79, p = 0.028) also tend to increase with size (Fig. 15).

Large specimens are thus represented by complete shells that are frequently encrusted and bored on external surfaces and preferentially coated by ferromanganese oxides but rarely infested by borers or encrusters on internal surfaces (Fig. 15).

DISCUSSION

Preservation of articulated shells

Low frequencies of altered shells in a DA can reflect either limited time-averaging and/or limited baseline alteration rate or total disintegration rate of brachiopod remains. The first factor is typically invoked in taphonomic or oceanographic studies focusing on continental shelf or slope environments subjected to variability in sedimentation (Best & Kidwell 2000; Powell *et al.* 2011*a*, 2011*b*) whereas the second factor is invoked in deep-sea studies where sedimentation is negligible (Thunell 1976; Le & Shackleton 1992; Suárez-Ibarra *et al.* 2021). High variability in alteration, with a mixture of articulated and disarticulated valves, is an expected outcome of background taphonomic processes that tend to be stochastic and patchy (i.e. bioerosion, encrustation or bioturbation), and some shells can be locally protected if buried by deep, non-local burial whereas others can remain exposed or are repeatedly buried and exhumed for long durations.

On the one hand, high abundance of articulated shells with fragile loops (Figs 8, 9) in the upper centimetres of a seabed at mid-bathyal depths in the Bari Canyon, without internal borers or encrusters, can be explained by scenarios invoking rapid burial: (1) exposure of skeletal remains in the TAZ is short owing to fast sedimentation, leading to permanent burial (obrution) of well-preserved and weakly time-averaged assemblages that can be comparable to censuses of living assemblages (Hallam 1972; Kidwell 1997; Feldman 2005; Brett *et al.* 2012); or (2) exposure of shells in the TAZ is short but not in steady

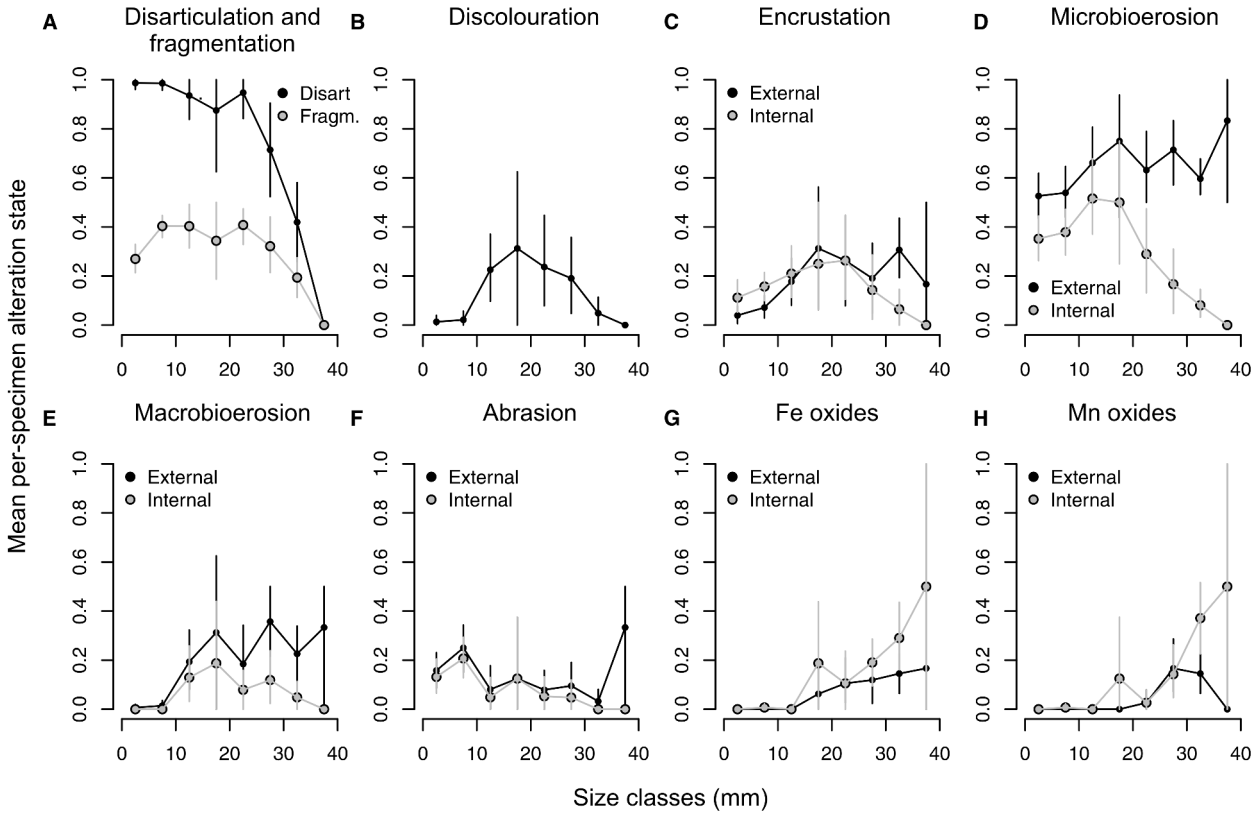

FIG. 15. Size dependency of alteration in *G. vitreus* on internal (grey) and external surfaces (black), with mean alteration per size class, with brachiopod specimens binned into 5 mm-size classes (using ventral valve length). A, disarticulation and fragmentation. B, discolouration. C, encrustation. D, microbioerosion, E, macrobioerosion. F, abrasion. G, Fe oxide coatings. H, Mn oxide coatings. Larger specimens are more frequently articulated, discoloured, and coated with Mn and Fe oxides than smaller specimens. Biotic infestation of interiors by encrusters and borers shows a conspicuous non-monotonic relationship with size, peaking at intermediate sizes, but decreasing with size in larger specimens. This pattern reflects the effect of the sediment fill of larger shells that prohibits the internal colonization of dead articulated shells.

state when conditions with fast sedimentation are followed by shell exhumation and sediment winnowing, leading to highly time-averaged assemblages formed by young shells mixed with old and recently exhumed, still well-preserved shells. On the other hand, high abundance of articulated shells with fragile loops can occur when exposure of shells in the TAZ is long but rates of disarticulation and valve disintegration are low, for example, owing to reduced flux of particulate organic matter to the seafloor, limiting carbonate dissolution driven by organic matter degradation in sediment, but also leading to food limitation of biomixers, bioirrigators and durophagous predators. This third scenario thus produces highly time-averaged assemblages with a significant proportion of well-preserved articulated shells.

Several lines of evidence indicate that the third pathway, without rapid burial but with slow disarticulation and disintegration, is more probable than the first two pathways with permanent or temporary burial. First, the co-occurrence of articulated shells with multi-centennial to millennial ages indicates that rapid burial by permanently high sedimentation rates is unlikely at this location, although the repeated phases of burial, winnowing and sediment erosion can lead to low net sedimentation rate. In any case, the DA with articulated shells and complete loops clearly does not reflect a single snapshot assemblage with limited time averaging.

Second, the extensive valve infestation by clionaid sponges (penetrating from the external surfaces, with internal valve surfaces rarely thickened in response to borings) and commissure-crossing encrusters on articulated shells demonstrate that external surfaces of the brachiopod shells were colonized post mortem. Internal borings that penetrate across the whole thickness of a valve from the exterior can remain unhealed on internal surfaces, as observed in live-collected bivalves (Lazo 2004). Intensely-bored segments (especially in umbonal parts) of some shells, however, led to a collapse of valve walls (Fig. 4A, B), indicating that shells were mainly bored by sponges after death.

Third, shells immediately buried in situ by episodic events or buried after short-term transport into the subsurface zones typically remain empty, incompletely filled by sediment and/or filled by cement (Graziano *et al.* 2006; Harper & Pickerill 2008; Baeza-Carratala *et al.* 2014). Such preservation contrasts with shells that can be filled with sediment when exposed at the sediment–water interface for longer durations (Seilacher 1968; Holland 1988). Such process may be associated with infestation of internal surfaces by borers or encrusters and by disintegration of lophophore supports. As most shell interiors were filled with sediment, the external surfaces of articulated shells were thus exposed to sediment input at the sediment–water interface. However, their interiors and lophophore supports remained protected, indicating that the rate of filling was very fast.

Fourth, the high frequency of Fe and Mn oxides on internal surfaces along edges of articulated shells and their presence at internal terminations of borings or in punctal pores indicates that the suboxic/oxic fronts were located at the interface between sediment infills enclosed within shells and valve internal surfaces. Dissolved iron or manganese can accumulate in suboxic, non-sulfidic zones, with metal reduction driven by degradation of organic matter within shells (Froelich *et al.* 1979; Kasten *et al.* 1998; Böhm & Brachert 1993; Jakubowicz *et al.* 2014; Guido *et al.* 2016), and precipitation at the redox fronts can be mediated by manganese- and iron-oxidizing bacteria (Thamdrup *et al.* 1994; Préat *et al.* 2006; Ferretti *et al.* 2012). Therefore, the redox fronts where Mn and Fe oxides precipitated were located within shells, and thus close to the sediment–water interface. This scenario is comparable to spatially-heterogeneous redox fronts that form when fluxes with dissolved iron or manganese are triggered by concentrations of decaying and patchily-distributed labile organic matter (Kalhorn & Emerson 1984; Gioncada *et al.* 2018) or when suboxic sediments lining borings or burrows are ventilated by oxic waters (Wetzel 2008; Ortiz Kfouri *et al.* 2021). Although ferromanganese coatings tend to form very slowly in deep-sea environments (approximately a few millimetres per million years; Hein & Koschinsky 2014), the postbomb ages of two shells with conspicuous Mn oxides indicate that their precipitation on internal surfaces of valves inside the brachiopod shells, as observed here, can be relatively fast: less than few years or decades (e.g. Usui *et al.* 2020). Therefore, to conclude, a subset of articulated shells was filled with sediment when exposed at or close to the sediment–water interface, either via pedicle opening or along a commissure of gaping valves.

Disarticulation and disintegration rates

Well-preserved shells of *G. vitreus* at the sampling station contrast with shallower DAs of *G. vitreus* characterized by rare articulated specimens and high proportion of worn fragments (Caulet 1972; Llompart 1988; Emig 1990). They also contrast with accumulations of other brachiopods found on temperate or tropical shelves and characterized by the lack of articulated shells with complete loops (Collins 1986; Daley 1993; Carroll *et al.* 2003; Tomašových & Rothfus 2005; Rodland *et al.* 2006, 2014; Tomašových & Zuschin 2009; Simões *et al.* 2007*a*, 2007*b*, 2009; Rodrigues & Simões 2010; Tomašových & Kidwell 2017). Therefore, both shell disarticulation and valve disintegration rates at the sediment–water interface are surprisingly low in the mid-bathyal environments of the Bari Canyon,

in contrast to taphonomically harsh conditions on the shelf or in the upper bathyal region in other locations in the Mediterranean Sea.

Although valve fragmentation can precede disarticulation, as was observed in one specimen of *G. vitreus*, disarticulation represents a first step in most pathways towards disintegration, followed by alteration and fragmentation of disarticulated valves (with thick umbonal relicts representing the last stages of disintegration), resulting in heavily altered specimens that can no longer be identified to species level. Therefore, the disarticulation rate is expected to be faster than overall disintegration rate. In theory, the vast majority of disarticulated valves can disintegrate rapidly and may not be preserved as identifiable remains if disintegration proceeds very fast following shell disarticulation. Such a pathway would generate a high frequency of articulated shells in the *G. vitreus* DA (>50% in some age cohorts). The *G. vitreus* fragments with thick umbonal regions and robust hinge plates, however, accrue diverse taphonomic signatures and are rather highly durable as evidenced by very low rates of disintegration of both smaller and larger *G. vitreus* specimens. The total disintegration rates are lower by a factor of 2 to 10 relative to the disarticulation rate. Disarticulated valves are thus unlikely to be under-represented in DAs when half-lives of valves are longer than half-lives of articulated shells. The high durability of disarticulated valves suggests that the high contribution of articulated specimens to the total assemblage directly mirrors the low rate of disarticulation occurring over multiple centuries. Under the disarticulation half-life of 200 years, *c.* 18% of shells will remain articulated after 500 years, and *c.* 3% of shells will still remain articulated after 1000 years. A shorter disarticulation half-life would produce unrealistically-high estimates of brachiopod population density (Fig. 2F), significantly exceeding annual density of 1000 individuals/m^2. Transport of shells from other habitats can concentrate and spatially-average shells at the sampled site, but the markedly bimodal size-frequency distribution or the lack of the bias in the ratio of ventral and dorsal valves in larger specimens indicate the lack of any significant sorting that would be predicted to occur if currents or downslope gravity flows concentrate or sort coarse skeletal remains such as brachiopod shells (Simões *et al.* 2005).

Sediment trapping as a mechanism preventing disarticulation and loop fragmentation

The cyrtomatodont hinge of *G. vitreus* with interlocked teeth and sockets increases the potential for the preservation of articulated shells relative to the non-interlocking (deltidiodont) hinge of other brachiopods (Brett & Bordeaux 1991; Li *et al.* 2016). However, first, this interlocking effect is not sufficient to prevent disarticulation of brachiopod shells in DAs on present-day, mainly temperate shelves. Second, even in the absence of disarticulation, the preservation of loops in taphofacies not generated by episodic burial requires that *G. vitreus* shells were not exposed to internal settlement by borers or cavity-dwelling organisms (that would lead to deterioration and fragmentation of loops formed exclusively by the secondary, organic-rich fibrous layer) or to any significant movements by bulldozing or burrowing organisms that would lead to disarticulation. Internal colonization of articulated shells of brachiopods was also documented in the fossil record when they were entrapped in sponge–microbial or coral–microbial framework and thus remained exposed to cryptobionts (Remia & Taviani 2005; Tomašových *et al.* 2006; Lee *et al.* 2016; Park *et al.* 2017).

A higher alteration of external surfaces relative to internal surfaces is a parsimonious expectation because external damage to epifaunal shells by borers or encrusters (or parasitic spionid polychaetes; Rodrigues 2007; Rodrigues *et al.* 2008) can occur during the lifetime of the brachiopod. Residence time of dead calcitic shells in the TAZ, however, still significantly exceeds the lifespan of living brachiopod individuals and the difference in preservation between external and internal surfaces is generally rapidly minimized in DAs of epifaunal species (Kidwell *et al.* 2001). The persistence of external–internal differences in alteration affecting old articulated shells is thus rather a diagnostic feature of unique pathways occurring in a TAZ where hinges remained interlocked and shell interiors remained closed and protected, with filling rates exceeding the rate of disarticulation or internal colonization of shells by cavity-dwelling cryptobionts. Although the size of the pedicle opening or of the gap between the valves can limit larval colonization of shell interiors, such limitation is contradicted by the observation that most shells were completely filled with sediment. If dead shells are oriented with umbo downwards (especially when the posterior region is thick as in *G. vitreus*), the anterior margin is not constrained and can gape within the limit allowed by interlocked valves.

We propose that trapping of sediment by closed or gaping shells can be one of the key processes that delays or inhibits disarticulation and stops the internal taphonomic clock for several centuries or even a few millennia because: (1) internal surfaces are pristine or unaltered in shells of *G. vitreus*; (2) these articulated shells display signs of extensive post-mortem bioerosion on external surfaces (comparable to alteration levels observed in disarticulated valves); and (3) internal lophophore support structures (loops) remain preserved in shells that resided in the TAZ for more than several centuries. Initially empty shells of dead brachiopods with a pedicle foramen and a limited opening between the two gaping but still

interlocked valves can over-collect sedimentary particles that float in suspension around the shells or are brought by currents (Seilacher 1968; Gardner 1980; Holland 1988). The gape angle of valves of cyrtomatodont brachiopods that is allowed by the hinge (prior its breakage) tends to be limited to <15° (Carlson 1989). Although this gape angle will increase with increasing hinge deterioration (Daley 1993), the limited gape in dead shells with well-preserved hinge can simultaneously allow for sediment filling but also for some protection against subsequent sediment winnowing and settlement of cryptobionts. Bottom currents tend to scour sediment around the up-current sides of dead shells, forming depressions into which shells can topple or slide, eventually burying them at the sediment–water interface (Alexander 1984; Messina & LaBarbera 2004). If sediment filling occurs at a rate that exceeds internal deterioration of loops inside the shells by cryptobionts, larger shells filled by sediment will be protected against cavity-dwellers and will be more resistant against reworking relative to empty shells. This shell-filling by sediment thus delays the taphonomic clock in shell interiors.

Sediment infilling of shells, however, is insufficient for long-term inhibition of disarticulation under extensive physical or biotic mixing of sediment, and conditions that minimize physical or biotic reworking in the Bari Canyon are probably necessary for the long-term preservation of articulated shells. Although the Bari Canyon environments are exposed to significant input of particulate organic matter sourced from the outer shelf and carried away by cascading currents, with intense bioturbation (Sanfilippo *et al.* 2013; Angeletti *et al.* 2014), the substrates are mixtures of soft sediment, coral rubble and hardground crusts, with high abundance of sediment-stabilizing epifaunal communities. Such conditions may generally lead to smaller depths and rates of mixing and irrigation relative to those observed on continental shelves.

Post-disarticulation pathways

The high abundance of juvenile brachiopods in DAs observed in live–dead analyses tends to be driven by high input of recently dead cohorts that were not subjected to disintegration by predators or had not yet degraded after they died (Noble & Logan 1981; Tomašových 2004; Pruden *et al.* 2018). The age-dated subset shows, however, that the small specimens of *G. vitreus* are as old as the larger specimens (Fig. 2G, H) and the peak in abundance of juveniles does not simply reflect a recent pulse in juvenile mortality. Although disintegration half-life of the smaller specimens is shorter than the half-life for larger shells, juveniles also disintegrate at a slow (multi-centennial) rate and are durable enough to accrue bioerosion, encrustation, discolouration or staining. The cohort-level taphonomic clock and multivariate analyses indicate that even sediment-filled shells eventually disarticulate and disintegrate by sponge bioerosion (with *Entobia* contributing to bioerosion observed in other brachiopods, Taddei Ruggiero & Bitner 2007; Bromley *et al.* 2008; Taddei Ruggiero & Raia 2010), wear related to exhumation, and/or by collapse of the secondary layer along the anterior margins (Gaspard 1989; Emig 1990) when residence time of specimens in the TAZ increases beyond a few millennia and both small and large specimens progress towards more worn and stained states. In spite of the differences in the intensity of disarticulation and alteration between the bathyal DAs in the Bari Canyon with well-preserved articulated shells and shallower environments with poorly-reserved disarticulated valves and fragments, the resulting time averaging in these environments attains similar, millennial scales (Table 2; Carroll *et al.* 2003; Krause *et al.* 2010; Tomašových & Kidwell 2017). This lack of differences may occur because time averaging in surface DAs is not simply limited by disintegration rate but is also determined by the rate at which shells can bypass the TAZ and by other early-diagenetic mechanisms that lead to alteration but can slow down overall disintegration.

Clay coatings (with dissolved coccoliths) and micrite cements, both contributing to brownish discolouration, occur on fragments older than *c.* 500 years and are typical of very old fragments (>2000 years). The co-occurrence of clay coatings and cements indicates that discoloured valves were confined to reducing conditions for long durations, triggering small-scale calcite dissolution in undersaturated pore waters, but locally also leading to precipitation of thin micrite cements. Very old, early Holocene or Pleistocene aragonitic skeletal remains in bathyal DAs are also typically stained and carry diverse early-diagenetic signatures on firm- or hardgrounds (Noé *et al.* 2006; Rivers *et al.* 2007; Freiwald *et al.* 2009; Angeletti & Taviani 2011, 2015; Tomašových *et al.* 2016*b*; Grun *et al.* 2020). Some worn, discoloured, and micritized valve fragments are encrusted by well-preserved foraminifers not affected by staining, indicating that they were exhumed from subsurface zones back to the sediment–water interface (Fig. 10H, I, K, L). To conclude, the taphonomic pathways of *G. vitreus* initially bifurcated at the time of disarticulation, separating the post-mortem fates of: (1) articulated shells that were rapidly filled by sediment and were protected from internal alteration but also from exhumation or displacements and could endure long exposure in the TAZ (Fig. 16A); and (2) shells that remained empty for a longer time or small shells rapidly filled with sediment, but possessed of a weak hinge, that were subjected to disarticulation (Fig. 16B). These two

TABLE 2. Estimates of time-averaging (IQR, interquartile age range) of brachiopods collected in surface death assemblages.

Region	Species	Station	N	IQR (years)	Water depth (m)	References
SE Brazilian Bight	*Bouchardia rosea*	Unatuba Bay 1	32	5472	30	Krause *et al.* (2010)
SE Brazilian Bight	*Bouchardia rosea*	Ubatuba Bay 9	71	1577	10	Carroll *et al.* (2003); Krause *et al.* (2010)
SE Brazilian Bight	*Bouchardia rosea*	Ubatumirim 1	19	225	5.7	Carroll *et al.* (2003)
SE Brazilian Bight	*Bouchardia rosea*	Ubatumirim 2	20	264	22.8	Carroll *et al.* (2003)
SE Brazilian Bight	*Bouchardia rosea*	Ilha das Couves	21	635	15.8	Carroll *et al.* (2003)
Southern California Bight	*Laqueus erythraeus*	Palos Verdes Shelf-0C	60	200	61	Tomašových & Kidwell (2017)
Southern California Bight	*Laqueus erythraeus*	Palos Verdes Shelf-10C	60	1974	61	Tomašových & Kidwell (2017)
Southern California Bight	*Laqueus erythraeus*	Palos Verdes Shelf-4134	39	1073	78	Tomašových & Kidwell (2017)
Southern California Bight	*Laqueus erythraeus*	Santa Monica Bay-24 205	31	1041	81	Tomašových & Kidwell (2017)
S Adriatic Sea	*Gryphus vitreus*	Bari Canyon-POS514-14	92	1249	580	This study

N, number of age-dated specimens.

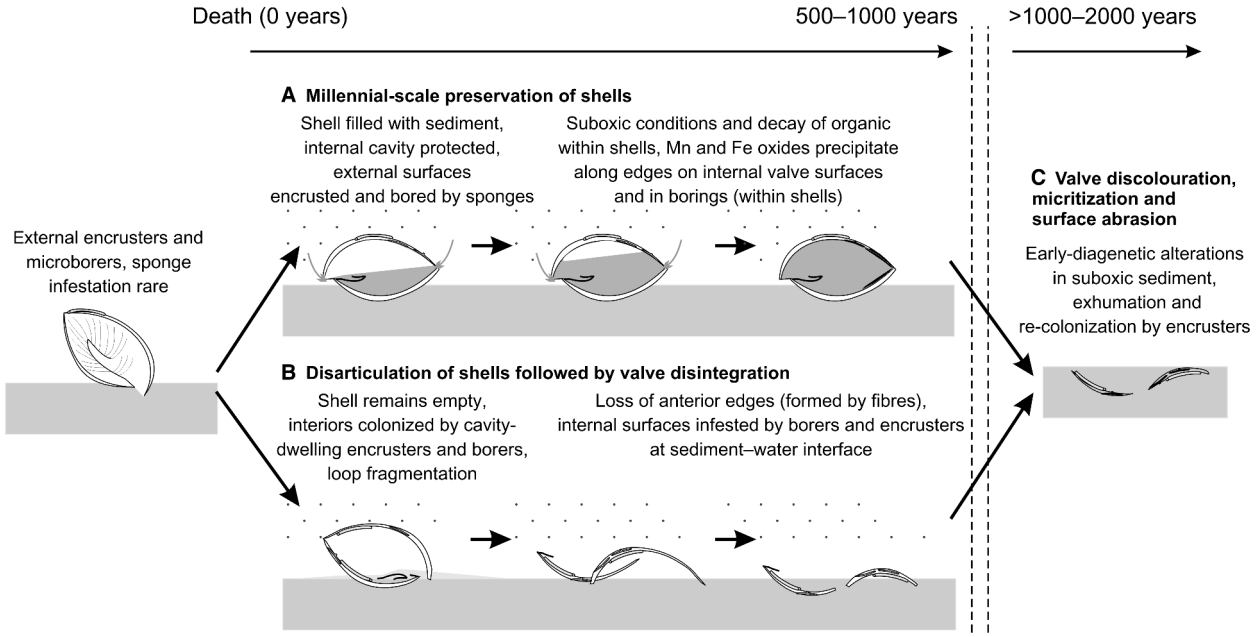

FIG. 16. Preservation pathways of *G. vitreus* in the TAZ (under conditions with sufficient amount of suspended particulate organic matter or sediment that can be trapped by shells). Shell disarticulation at the sediment–water interface (in the TAZ) is a stochastic process determined by the rate of shell infilling by sediment. Shells are externally encrusted and microbored during life (with rare sponge infestation). A high abundance of articulated shells enters into death assemblages (assuming durophagous predation is limited). Shells can initially be subjected to one of two pathways (A, B) that eventually converge to the same final pathway (C). A, shells are rapidly filled by sediment from suspension or brought by currents (grey arrows), via pedicle opening or via gaping valves or both, before they can be colonized by cavity-dwelling borers or encrusters and/or before they disarticulate. Sediment infill prevents loop fragmentation. Dead sediment-filled shells located at the sediment–water interface are externally bored by sponges, encrusted by organisms crossing the commissure, and internally coated by Mn and Fe oxides at the oxic/suboxic fronts (black internal coatings along the anterior margin). This pathway allows multi-centennial residence of the *G. vitreus* dead shells in the surface TAZ. B, empty shells are internally infested by borers and encrusters and disarticulate and fragment at a rate that exceeds their rate of filling by sediment. C, at time scales exceeding *c.* 1000–2000 years, most specimens are represented by discoloured and abraded fragments. Regardless of conditions at the sediment–water interface, long-term exposure thus leads to shell disarticulation and valve deterioration by bioerosion, softening of the secondary shell, and abrasion.

states eventually converge and lead to worn, bored and discoloured fragments (Fig. 16C).

Present-day bathyal analogue for taphonomic pathways on shelves prior to the Mesozoic Marine Revolution

Carbonate disintegration may be slower in present-day bathyal environments than on shelves owing to multiple phenomena that are related to a bathymetric decline in predation (Walker *et al.* 2002); bioerosion intensity (Wisshak *et al.* 2005; Tomašových & Zuschin 2009; Walker *et al.* 2011), export of organic matter (reducing dissolution rate, Aller 1982; Archer 1991; Reimers *et al.* 1992; Mekik *et al.* 2002) and bioturbation rate (Boudreau 1994; Middelburg *et al.* 1997; Henderson *et al.* 1999; Smith *et al.* 2000; Meile & Van Cappellen 2003). Although durophagous predation, grazing and bioturbation intensified to some degree during the Triassic and Jurassic, and plankton have diversified since the Middle Jurassic (Kowalewski *et al.* 1998; Harper & Wharton 2000; Hautmann 2004; Radley 2010; Schweitzer & Feldman 2010; Bardhan *et al.* 2012; Salamon *et al.* 2012; Suchéras-Marx *et al.* 2019; Tackett & Tintori 2019; Manojlovic & Clapham 2021; Buatois *et al.* 2022; Cueille *et al.* 2020), these processes were probably less effective on shelves prior to the main Cretaceous phase of the MMR that intensified both shell fragmentation by durophagous predators and post-mortem deterioration of organic and carbonate materials in the TAZ.

Even when brachiopods are numerically abundant on Holocene–Anthropocene continental shelves, the abundance of articulated and complete valves of epifaunal brachiopods is rapidly reduced in DAs under the taphonomic conditions typical of present-day continental shelves. Although the rates and intensity of biotic interactions decline with decreasing temperature, and cold-temperate conditions in bathyal environments can thus be characterized by their low intensity, seawater temperatures also remain within 12.5–14°C at shallower locations in the western Mediterranean Sea where *G. vitreus* disarticulation and alteration rates are faster, and examples of the fast deterioration of brachiopod shells have been documented in shallow-water conditions with temperatures <10°C (Daley 1993; Tomašových 2004). Therefore, the high alteration rates observed in shelf environments cannot be explained by bathymetric gradients in seawater temperature. Taphonomic pathways determining the quality of preservation of brachiopod shells in modern shallow-marine DAs are thus probably distinct from pathways that characterized similar environments prior to the MMR. Preservation of shell-rich brachiopod assemblages in Cenozoic shelf deposits is also frequently characterized by high abundance of disarticulated and fragmented valves (Reolid *et al.* 2012; García-Ramos & Zuschin 2019), unless entombed by episodic burial (that will tend to lead to the preservation of incompletely-filled, empty or cement-filled shells; Skompski *et al.* 2018). The taphonomic clock is thus typically accelerated in shallow marine environments; most destructive alteration occurs early, and age cohorts that are decades or centuries old may not differ in alteration (Agiadi *et al.* 2021; Tomašových *et al.* 2022*c*). Slow disarticulation and fragmentation of brachiopods in the Bari Canyon contradicts this dynamic, leading to a delayed taphonomic clock (Fig. 14A). DAs with articulated shells of *G. vitreus*, with similar preservation with rusty or blackish oxide coatings were also documented at similar bathyal depths in the Ionian Sea at Santa Maria di Leuca coral province (Rosso *et al.* 2010), indicating that these conditions are not unique to the Bari Canyon. We suggest that in contrast to the pre-MMR conditions, this low-intensity taphonomic dynamic detected in bathyal environments is rare in the seabeds of present-day shelves, unless bioturbation is reduced due to anthropogenic impacts.

CONCLUSION

We describe a preservation pathway in which dead brachiopod shells exposed at the sediment–water interface trap sediment significantly, stopping their disarticulation and other sources of alteration in their interiors for several centuries (with some shells remaining articulated for *c.* 1500 years) in deeper bathyal environments not subjected to extensive bioturbation or durophagous predation. This pathway thus allows for the preservation of articulated shells in the absence of episodic burial and may be a unique testament of generally low intensity of biotic interactions that directly or indirectly contribute to skeletal alteration and disintegration. Although the multimillennial residence time in the TAZ eventually leads to disarticulation owing to bioerosion and other sources of damage, the high frequency of articulated, sediment-filled shells of *G. vitreus* with well-preserved loops in surface DAs in the Bari Canyon still markedly contrasts with abundance of disarticulated and worn brachiopods on present-day shelves. Although juveniles (<20 mm in length) are characterized by a shorter disintegration half-life (*c.* 500 years) compared to adults (*c.* 1700 years), their half-life is still relatively long to allow for the accumulation of small-sized individuals in time-averaged DAs. We suggest that the preservation of sediment-filled articulated shells of brachiopods with well-preserved loops in bathyal environments of the Bari Canyon is a signature of mild conditions in the TAZ that mimics taphonomic attributes of brachiopod shell accumulations in the Palaeozoic or the Mesozoic stratigraphic record: articulated shells

were not buried rapidly but resided in a relatively well-preserved preservation state at the sediment–water interface for long durations (i.e. several decades or centuries).

Acknowledgements. We thank Sally Thomas, Marcello G. Simões and one anonymous referee for helpful and critical comments. We thank all the members of Poseidon cruise No. 514, particularly chief scientist Hartmut Schulz, Petra Heinz and Tobias B. Grun for help with sampling. We are also grateful to Filip Šetena and Angela Scheidl for their help with sample sorting, Jordon Bright for preparing ^{14}C targets, and Jan Steger for help with molluscan identification. This research was supported by the Slovak Research and Development Agency (grant no. APVV 17-0555), and the Slovak Scientific Grant Agency (grant no. VEGA 2/0169/19). Shell dating was supported by a grant of the University of Vienna (Austria) to MZ.

Author contributions. **Conceptualization** A Tomašových (AT), DA García-Ramos (DAG-R), JH Nebelsick (JHN), M Zuschin (MZ); **Data Curation** AT, DAG-R, R Nawrot (RN), MZ; **Formal Analysis** AT; **Funding Acquisition** JHN, MZ; **Writing – Original Draft Preparation** AT; **Writing – Review & Editing** AT, DAG-R, RN, JHN, MZ.

DATA ARCHIVING STATEMENT

Raw data with taphonomic scores, post-mortem ages and sizes of *Gryphus vitreus* and R language script for analyses are available in the Dryad Digital Repository: https://doi.org/10.5061/dryad.8w9ghx3qb

Editor. Nadia Santodomingo

REFERENCES

ABDELHADY, A. A. and FÜRSICH, F. T. 2014. Macroinvertebrate palaeo-communities from the Jurassic succession of Gebel Maghara (Sinai, Egypt). *Journal of African Earth Sciences*, **97**, 173–193.

AGIADI, K., AZZARONE, M., HUA, Q., KAUFMAN, D. S., THIVAIOU, D. and ALBANO, P. G. 2021. The taphonomic clock in fish otoliths. *Paleobiology*, **48**, 154–170.

ALBANO, P. G., HUA, Q., KAUFMAN, D. S., TOMAŠOVÝCH, A., ZUSCHIN, M. and AGIADI, K. 2020. Radiocarbon dating supports bivalve-fish age coupling along a bathymetric gradient in high-resolution paleoenvironmental studies. *Geology*, **48**, 589–593.

ALEXANDER, R. R. 1984. Comparative hydrodynamic stability of brachiopod shells on current-scoured arenaceous substrates. *Lethaia*, **17**, 17–32.

ALEXANDER, R. R. 1990. Disarticulated shells of Late Ordovician brachiopods: inferences on strength of hinge and valve architecture. *Journal of Paleontology*, **64**, 524–532.

ALEXANDER, R. R. and GIBSON, M. A. 1993. Paleozoic brachiopod autecology based on taphonomy: example from the Devonian Ross Formation of Tennessee (USA). *Palaeogeography, Palaeoclimatology, Palaeoecology*, **100**, 25–35.

ALLER, R. C. 1982. Carbonate dissolution in nearshore terrigenous muds: the role of physical and biological reworking. *Journal of Geology*, **90**, 79–95.

ALLMEN, K. VON, NÄGLER, T. F., PETTKE, T., HIPPLER, D., GRIESSHABER, E., LOGAN, A., EISENHAUER, A. and SAMANKASSOU, E. 2010. Stable isotope profiles (Ca, O, C) through modern brachiopod shells of *T. septentrionalis* and *G. vitreus*: implications for calcium isotope paleo-ocean chemistry. *Chemical Geology*, **269**, 210–219.

ANGELETTI, L. and TAVIANI, M. 2011. Entrapment, preservation and incipient fossilization of benthic predatory molluscs within deep-water coral frames in the Mediterranean Sea. *Geobios*, **44**, 543–548.

ANGELETTI, L., TAVIANI, M., CANESE, S., FOGLINI, F., MASTROTOTARO, F., ARGNANI, A., TRINCARDI, F., BAKRAN-PETRICIOLI, T., CEREGATO, A., CHIMIENTI, G. and MAČIĆ, V. 2014. New deep-water cnidarian sites in the southern Adriatic Sea. *Mediterranean Marine Science*, **15**, 263–273.

ANGELETTI, L., CANESE, S., FRANCHI, F., MONTAGNA, P., REITNER, J., WALLISER, E. O. and TAVIANI, M. 2015. The "chimney forest" of the deep Montenegrin margin, south-eastern Adriatic Sea. *Marine & Petroleum Geology*, **66**, 542–554.

ANGELETTI, L., PRAMPOLINI, M., FOGLINI, F., GRANDE, V. and TAVIANI, M. 2020. Cold-water coral habitat in the Bari Canyon System, Southern Adriatic Sea (Mediterranean Sea). 811–824. *In* HARRIS, P. and BAKER, E. (eds) *Seafloor geomorphology as benthic habitat*. Elsevier.

ARCHER, D. 1991. Modeling the calcite lysocline. *Journal of Geophysical Research: Oceans*, **96**, 17037–17050.

ASHTON-ALCOX, K. A., MORSON, J. M., POWELL, E. N., GIUS, J. E., MUNROE, D. M. and BUSHEK, D. 2021. Oyster recruitment and persistence on planted versus native substrate over 13 year in the Delaware Bay oyster fishery resource. *Journal of Shellfish Research*, **40**, 191–211.

BAEZA-CARRATALA, J. F., GIANNETTI, A., TENTMANCLUS, J. E. and JORAL, F. G. 2014. Evaluating taphonomic bias in a storm-disturbed carbonate platform: effects of compositional and environmental factors in Lower Jurassic brachiopod accumulations (eastern Subbetic Basin, Spain). *PALAIOS*, **29**, 55–73.

BAMBACH, R. K. 1993. Seafood through time: changes in biomass, energetics, and productivity in the marine ecosystem. *Paleobiology*, **19**, 372–397.

BARDHAN, S., CHATTOPADHYAY, D., MONDAL, S., DAS, S. S., MALLICK, S., ROY, A. and CHANDA, P. 2012. Record of intense predatory drilling from Upper Jurassic bivalves of Kutch, India: implications for the history of biotic interaction. *Palaeogeography, Palaeoclimatology, Palaeoecology*, **317**, 153–161.

BEST, M. M. and KIDWELL, S. M. 2000. Bivalve taphonomy in tropical mixed siliciclastic-carbonate settings. I. Environmental variation in shell condition. *Paleobiology*, **26**, 80–102.

BÖHM, F. and BRACHERT, T. C. 1993. Deep-water stromatolites and *Frutexites* Maslov from the Early and Middle Jurassic of S-Germany and Austria. *Facies*, **28**, 145–168.

BOUDREAU, B. P. 1994. Is burial velocity a master parameter for bioturbation? *Geochimica et Cosmochimica Acta*, **58**, 1243–1249.

BOULLIER, A., DELANCE, J. H., EMIG, C. C., D'HONDT, J. L., GASPARD, D. and LAURIN, B. 1986. Les populations de *Gryphus vitreus* (Brachiopoda) en Corse. Implications paléontologiques. *Biostratigraphie du Paléozoïque*, **4**, 179–196.

BRETT, C. E. and BORDEAUX, Y. L. 1991. Taphonomy of brachiopods from a Middle Devonian shell bed: implications for the genesis of skeletal accumulations. 219–232. *In* MACKINNON, D. I., LEE, D. E. and CAMPBELL, J. D. (eds) *Brachiopods through time*. A.A. Balkema.

BRETT, C. E., ZAMBITO, J. J. IV, SCHINDLER, E. and BECKER, R. T. 2012. Diagenetically-enhanced trilobite obrution deposits in concretionary limestones: the paradox of "rhythmic events beds". *Palaeogeography, Palaeoclimatology, Palaeoecology*, **367**, 30–43.

BROMLEY, R. G. and SURLYK, F. 1973. Borings produced by brachiopod pedicles, fossil and Recent. *Lethaia*, **6**, 349–365.

BROMLEY, R. G., WISSHAK, M., GLAUB, I. and BOTQUELEN, A. 2007. Ichnotaxonomic review of dendriniform borings attributed to foraminiferans: *Semidendrina* igen. nov. 518–530. *In* MILLER, W. III (ed.) *Trace fossils: Concepts, problems, prospects*. Elsevier.

BROMLEY, R. G., BEUCK, L. and RUGGIERO, E. T. 2008. Endolithic sponge versus terebratulid brachiopod, Pleistocene, Italy: accidental symbiosis, bioclaustration and deformity. 361–368. *In* WISSHAK, M. and TAPANILLA, L. (eds) *Current developments in bioerosion*. Springer.

BUATOIS, L. A., CARMONA, N. B., CURRAN, H. A., NETTO, R. G., MÁNGANO, M. G. and WETZEL, A. 2016. The Mesozoic marine revolution. 19–134. *In* MANGANO, M. G. and BUATOIS, L. A. (eds) *The trace-fossil record of major evolutionary events*. Springer.

BUATOIS, L. A., MÁNGANO, M. G., DESAI, B., CARMONA, N. B., BURNS, F., MEEK, D. and EGLINGTON, B. 2022. Infaunalization and resource partitioning during the Mesozoic marine revolution. *Geology*, **50**, 786–790.

BUSH, S. L., SANTOS, G. M., XU, X., SOUTHON, J. R., THIAGARAJAN, N., HINES, S. K. and ADKINS, J. F. 2013. Simple, rapid, and cost effective: a screening method for ^{14}C analysis of small carbonate samples. *Radiocarbon*, **55**, 631–640.

CALLENDER, W. R., STAFF, G. M., PARSONS-HUBBARD, K. M., POWELL, E. N., ROWE, G. T., WALKER, S. E., BRETT, C. E., RAYMOND, A., CARLSON, D. D., WHITE, S. and HEISE, E. A. 2002. Taphonomic trends along a forereef slope: Lee Stocking Island, Bahamas. I. Location and water depth. *PALAIOS*, **17**, 50–65.

CARLSON, S. J. 1989. The articulate brachiopod hinge mechanism: morphological and functional variation. *Paleobiology*, **15**, 364–386.

CARTES, J. E., MAYNOU, F., FANELLI, E., ROMANO, C., MAMOURIDIS, V. and PAPIOL, V. 2009. The distribution of megabenthic, invertebrate epifauna in the Balearic Basin (western Mediterranean) between 400 and 2300 m: environmental gradients influencing assemblages composition and biomass trends. *Journal of Sea Research*, **61**, 244–257.

CARROLL, M., KOWALEWSKI, M., SIMÕES, M. G. and GOODFRIEND, G. A. 2003. Quantitative estimates of time-averaging in terebratulid brachiopod shell accumulations from a modern tropical shelf. *Paleobiology*, **29**, 381–402.

CAULET, J. P. 1972. Les sédiments organogènes du précontinent Algérien. *Mémoires du Muséum National d'Histoire Naturelle, Nouvelle Series, Serie C*, **25**, 1–295.

CHEN, J., CHEN, Z. Q. and TONG, J. N. 2010. Palaeoecology and taphonomy of two brachiopod shell beds from the Anisian (Middle Triassic) of Guizhou, Southwest China: recovery of benthic communities from the end-Permian mass extinction. *Global & Planetary Change*, **73**, 149–160.

CHERNS, L. and WRIGHT, V. P. 2009. Quantifying the impacts of early diagenetic aragonite dissolution on the fossil record. *PALAIOS*, **24**, 756–771.

CHERNS, L., WHEELEY, J. R. and WRIGHT, V. P. 2008. Taphonomic windows and molluscan preservation. *Palaeogeography, Palaeoclimatology, Palaeoecology*, **270**, 220–229.

CLAPHAM, M. E., BOTTJER, D. J., POWERS, C. M., BONUSO, N., FRAISER, M. L., MARENCO, P. J., DORNBOS, S. Q. and PRUSS, S. B. 2006. Assessing the ecological dominance of Phanerozoic marine invertebrates. *PALAIOS*, **21**, 431–441.

COLANTONI, P. and GALLIGNANI, P. 1978. Quaternary evolution of the continental shelf off the coast of Bari (South Adriatic Sea): shallow seismic, sedimentological and faunal evidences. *Géologie Méditerranéenne*, **5**, 327–338.

COLANTONI, P., NOTO, P. and TAVIANI, M. 1975. Prime datazioni assolute di una fauna fossile a *Pseudamussium septemradiatum* dragata nel basso Adriatico. *Giornale di Geologia*, **40**, 133–140.

COLLINS, M. J. 1986. Post mortality strength loss in shells of the Recent articulate brachiopod *Terebratulina retusa* (L.) from the west coast of Scotland. *Biostratigraphie du Paléozoïque*, **4**, 209–218.

COPPER, P. 1997. Articulate brachiopod shellbeds: Silurian examples from Anticosti, eastern Canada. *Geobios*, **30**, 133–148.

CUEILLE, M., GREEN, E., DUFFIN, C. J., HILDEBRANDT, C. and BENTON, M. J. 2020. Fish and crab coprolites from the latest Triassic of the UK: from Buckland to the Mesozoic Marine Revolution. *Proceedings of the Geologists' Association*, **131**, 699–721.

CUMMINS, H., POWELL, E. N., STANTON, R. J. Jr. and STAFF, G. 1986. The rate of taphonomic loss in modern benthic habitats: how much of the potentially preservable community is preserved? *Palaeogeography, Palaeoclimatology, Palaeoecology*, **52**, 291–320.

DALEY, G. M. 1993. Passive deterioration of shelly material: a study of the recent eastern Pacific articulate brachiopod *Terebratalia transversa* Sowerby. *PALAIOS*, **8**, 226–232.

DATTILO, B. F., BRETT, C. E., TSUJITA, C. J. and FAIRHURST, R. 2008. Sediment supply versus storm winnowing in the development of muddy and shelly interbeds from the Upper Ordovician of the Cincinnati region, USA. *Canadian Journal of Earth Sciences*, **45**, 243–265.

DATTILO, B. F., BRETT, C. E. and SCHRAMM, T. J. 2012. Tempestites in a teapot? Condensation-generated shell

beds in the Upper Ordovician, Cincinnati Arch, USA. *Palaeogeography, Palaeoclimatology, Palaeoecology*, **367**, 44–62.

DAVIES, D. J., POWELL, E. N. and STANTON, R. J. Jr. 1989. Relative rates of shell dissolution and net sediment accumulation-a commentary: can shell beds form by the gradual accumulation of biogenic debris on the sea floor? *Lethaia*, **22**, 207–212.

D'HONDT, J. L. 1984. Bryozoaires épibiontes sur le brachiopode articulé *Gryphus vitreus* (Born, 1778) en mer Méditerranée occidentale (Corse). *Vie et Milieu/Life & Environment*, **34**, 27–33.

DOLENEC, T. 2003. Ferromanganese coated structures from the Jabuka Pit (Central Adriatic): mineralogical, geochemical and genetic considerations. *Croatica Chemica Acta*, **76**, 207–215.

D'ONGHIA, G., CAPEZZUTO, F., CARDONE, F., CARLUCCI, R., CARLUCCIO, A., CHIMIENTI, G., CORRIERO, G., LONGO, C., MAIORANO, P., MASTROTOTARO, F. and PANETTA, P. 2015. Macro-and megafauna recorded in the submarine Bari Canyon (southern Adriatic, Mediterranean Sea) using different tools. *Mediterranean Marine Science*, **16**, 180–196.

DEXTER, T. A., KAUFMAN, D. S., KRAUSE, R. A., WOOD, S. L. B., SIMÕES, M. G., HUNTLEY, J. W., YANES, Y., ROMANEK, C. S. and KOWALEWSKI, M. 2014. A continuous multi-millennial record of surficial bivalve mollusk shells from the São Paulo Bight, Brazilian shelf. *Quaternary Research*, **81**, 274–283.

EMIG, C. C. 1985. Distribution et synécologie des fonds à *Gryphus vitreus* (Brachiopoda) en Corse. *Marine Biology*, **90**, 139–146.

EMIG, C. C. 1987. Offshore brachiopods investigated by submersible. *Journal of Experimental Marine Biology & Ecology*, **108**, 261–273.

EMIG, C. C. 1989. Distributional patterns along the Mediterranean continental margin (Upper Bathyal) using *Gryphus vitreus* (Brachiopoda) densities. *Palaeogeography, Palaeoclimatology, Palaeoecology*, **71**, 253–256.

EMIG, C. C. 1990. Examples of post-mortality alteration in Recent brachiopod shells and (paleo)ecological consequences. *Marine Biology*, **104**, 233–238.

EMIG, C. C. and GARCÍA-CARRASCOSA, M. A. 1991. Distribution of *Gryphus vitreus* (Born, 1778) (Brachiopoda) on transect P2 (Continental margin, French Mediterranean coast) investigated by submersible. *Scientia Marina*, **55**, 385–388.

FANTASIA, A., MATTIOLI, E., SPANGENBERG, J. E., ADATTE, T., BERNÁRDEZ, E., FERREIRA, J., THIBAULT, N., KRENCKER, F. N. and BODIN, S. 2022. The middle-late Aalenian event: a precursor of the Mesozoic Marine Revolution. *Global & Planetary Change*, **208**, 103705.

FELDMAN, H. R. 2005. Paleoecology, taphonomy, and biogeography of a *Coenothyris* community (Brachiopoda, Terebratulida) from the Triassic (Upper Anisian–Lower Ladinian) of Israel. *American Museum Novitates*, **2005**, 1–20.

FERRETTI, A., CAVALAZZI, B., BARBIERI, R., WESTALL, F., FOUCHER, F. and TODESCO, R. 2012. From black-and-white to colour in the Silurian. *Palaeogeography, Palaeoclimatology, Palaeoecology*, **367**, 178–192.

FLESSA, K. W., CUTLER, A. H. and MELDAHL, K. H. 1993. Time and taphonomy: quantitative estimates of time-averaging and stratigraphic disorder in a shallow marine habitat. *Paleobiology*, **19**, 266–286.

FREIWALD, A., BEUCK, L., RÜGGEBERG, A., TAVIANI, M. and HEBBELN, D. 2009. The white coral community in the central Mediterranean Sea revealed by ROV surveys. *Oceanography*, **22**, 58–74.

FROELICH, P., KLINKHAMMER, G. P., BENDER, M. L., LUEDTKE, N. A., HEATH, G. R., CULLEN, D., DAUPHIN, P., HAMMOND, D., HARTMAN, B. and MAYNARD, V. 1979. Early oxidation of organic matter in pelagic sediments of the eastern equatorial Atlantic: suboxic diagenesis. *Geochimica et Cosmochimica Acta*, **43**, 1075–1090.

FÜRSICH, F. T., BERNDT, R., SCHEUER, T. and GAHR, M. 2001. Comparative ecological analysis of Toarcian (Lower Jurassic) benthic faunas from southern France and east-central Spain. *Lethaia*, **34**, 169–199.

GAMULIN-BRIDA, H. 1973. Contribution aux recherches sur les biocoenoses benthiques de l'étage bathyal de la mer Adriatique. *Rapports et Procès-verbaux des Réunions Commission internationale pour l'Exploration scientifique de la Mer Méditerranée*, **21**, 691–693.

GAMULIN-BRIDA, H. 1983. La côte de Crna gora – une partie spécifique de la mer Adriatique a l'égard des biocénoses benthiques et leur protéction. *Studia Marina*, **13–14**, 205–214.

GARCÍA-RAMOS, D. A. and ZUSCHIN, M. 2019. High-frequency cycles of brachiopod shell beds on subaqueous delta-scale clinoforms (early Pliocene, south-east Spain). *Sedimentology*, **66**, 1486–1530.

GARDNER, W. D. 1980. Sediment trap dynamics and calibration: a laboratory evaluation. *Journal of Marine Research*, **38**, 17–39.

GASPARD, D. 1989. Quelques aspects de la biodégradation des coquilles de brachiopodes; conséquences sur leur fossilisation. *Bulletin de la Société Géologique de France*, **6**, 1207–1216.

GASPARD, D. 2011. Endolithic algae, fungi and bacterial activity in Holocene and Cretaceous brachiopod shells-diagenetic consequences. *Memoirs of the Association of Australasian Palaeontologists*, **41**, 327–337.

GASPARD, D., MARIN, F., GUICHARD, N., MOREL, S., ALCARAZ, G. and LUQUET, G. 2007. Shell matrices of Recent rhynchonelliform brachiopods: microstructures and glycosylation studies. *Earth & Environmental Science Transactions of the Royal Society of Edinburgh*, **98**, 415–424.

GIONCADA, A., GARIBOLDI, K., COLLARETA, A., CELMA, C. D., BOSIO, G., MALINVERNO, E., LAMBERT, O., PIKE, J., URBINA, M. and BIANUCCI, G. 2018. Looking for the key to preservation of fossil marine vertebrates in the Pisco Formation of Peru: new insights from a small dolphin skeleton. *Andean Geology*, **45**, 379–398.

GLOVER, C. P. and KIDWELL, S. M. 1993. Influence of organic matrix on the post-mortem destruction of molluscan shells. *Journal of Geology*, **101**, 729–747.

GORZELAK, P., SALAMON, M. A. and BAUMILLER, T. K. 2012. Predator-induced macroevolutionary trends in Mesozoic crinoids. *Proceedings of the National Academy of Sciences*, **109**, 7004–7007.

GRAZIANO, R., BUONO, G. and TADDEI RUGGIERO, E. 2006. Lower Toarcian (Jurassic) brachiopod-rich carbonate facies of the Gran Sasso range (central Apennines, Italy). *Bolletino della Societa Paleontologica Italiana*, **45**, 61–74.

GRINYÓ, J., GORI, A., GREENACRE, M., REQUENA, S., CANEPA, A., IACONO, C. L., AMBROSO, S., PURROY, A. and GILI, J. M. 2018. Megabenthic assemblages in the continental shelf edge and upper slope of the Menorca Channel, Western Mediterranean Sea. *Progress in Oceanography*, **162**, 40–51.

GRUN, T. B., MIHALJEVIĆ, M. and WEBB, G. E. 2020. Comparative taphonomy of deep-sea and shallow-marine echinoids of the genus *Echinocyamus*. *PALAIOS*, **35**, 403–420.

GUIDO, A., ROSSO, A., SANFILIPPO, R., RUSSO, F. and MASTANDREA, A. 2016. Frutexites from microbial/metazoan bioconstructions of recent and Pleistocene marine caves (Sicily, Italy). *Palaeogeography, Palaeoclimatology, Palaeoecology*, **453**, 127–138.

HALLAM, A. 1972. Models involving population dynamics. 62–80. *In* SCHOPF, T. J. M. (ed.) *Models in paleobiology*. Freeman Cooper & Co.

HARPER, D. A. and PICKERILL, R. K. 2008. Generation of brachiopod-dominated shell beds in the Miocene rocks of Carriacou, Lesser Antilles. *Geological Journal*, **43**, 573–581.

HARPER, E. M. and WHARTON, D. S. 2000. Boring predation and Mesozoic articulate brachiopods. *Palaeogeography, Palaeoclimatology, Palaeoecology*, **158**, 15–24.

HAUTMANN, M. 2004. Early Mesozoic evolution of alivincular bivalve ligaments and its implications for the timing of the 'Mesozoic marine revolution'. *Lethaia*, **37**, 165–172.

HEIN, J. R. and KOSCHINSKY, A. 2014. Deep-ocean ferromanganese crusts and nodules. 273–291. *In* HOLLAND, H. D. and TUREKIAN, K. K. (eds) *Treatise on geochemistry*, Second edition. Elsevier.

HELIASZ, Z. and RACKI, G. 1980. Ecology of the upper Jurassic brachiopod bed from Julianka, Polish Jura Chain. *Acta Geologica Polonica*, **30**, 175–197.

HENDERSON, G. M., LINDSAY, F. N. and SLOWEY, N. C. 1999. Variation in bioturbation with water depth on marine slopes: a study on the Little Bahamas Bank. *Marine Geology*, **160**, 105–118.

HOLLAND, S. M. 1988. Taphonomic effects of sea-floor exposure on an Ordovician brachiopod assemblage. *PALAIOS*, **3**, 588–597.

JAKUBOWICZ, M., BELKA, Z. and BERKOWSKI, B. 2014. *Frutexites* encrustations on rugose corals (Middle Devonian, southern Morocco): complex growth of microbial microstromatolites. *Facies*, **60**, 631–650.

KALHORN, S. and EMERSON, S. 1984. The oxidation state of manganese in surface sediments of the deep sea. *Geochimica et Cosmochimica Acta*, **48**, 897–902.

KASTEN, S., FREUDENTHAL, T., GINGELE, F. X. and SCHULZ, H. D. 1998. Simultaneous formation of iron-rich layers at different redox boundaries in sediments of the Amazon deep-sea fan. *Geochimica et Cosmochimica Acta*, **62**, 2253–2264.

KFOURI, L. O., MILLO, C., DE LIMA, A. E., SILVEIRA, C. S., SANT'ANNA, L. G., MARINO, E., GONZÁLEZ, F. J., SAYEG, I. J., HEIN, J. R., JOVANE, L. and BERNARDINI, S. 2021. Growth of ferromanganese crusts on bioturbated soft substrate, Tropic Seamount, northeast Atlantic ocean. *Deep Sea Research Part I: Oceanographic Research Papers*, **175**, 103586.

KIDWELL, S. M. 1990. Phanerozoic evolution of macroinvertebrate shell accumulations: preliminary data from the Jurassic of Britain. *Paleontological Society Special Publications*, **5**, 309–327.

KIDWELL, S. M. 1997. Time-averaging in the marine fossil record: overview of strategies and uncertainties. *Geobios*, **30**, 977–995.

KIDWELL, S. M. and BRENCHLEY, P. J. 1994. Patterns in bioclastic accumulation through the Phanerozoic: changes in input or in destruction? *Geology*, **22**, 1139–1143.

KIDWELL, S. M. and BRENCHLEY, P. J. 1996. Evolution of the fossil record: thickness trends in marine skeletal accumulations and their implications. 290–336. *In* JABLONSKI, D., ERWIN, D. H. and LIPPS, J. H. (eds) *Evolutionary paleobiology*. University of Chicago Press.

KIDWELL, S. M., ROTHFUS, T. A. and BEST, M. M. 2001. Sensitivity of taphonomic signatures to sample size, sieve size, damage scoring system, and target taxa. *PALAIOS*, **16**, 26–52.

KIDWELL, S. M., BEST, M. M. and KAUFMAN, D. S. 2005. Taphonomic trade-offs in tropical marine death assemblages: differential time averaging, shell loss, and probable bias in siliciclastic vs. carbonate facies. *Geology*, **33**, 729–732.

KOLBE, S. E., ZAMBITO, J. J. IV, BRETT, C. E., WISE, J. L. and WILSON, R. D. 2011. Brachiopod shell discoloration as an indicator of taphonomic alteration in the deep-time fossil record. *PALAIOS*, **26**, 682–692.

KOSNIK, M. A., HUA, Q., JACOBSEN, G. E., KAUFMAN, D. S. and WÜST, R. A. 2007. Sediment mixing and stratigraphic disorder revealed by the age-structure of Tellina shells in Great Barrier Reef sediment. *Geology*, **35**, 811–814.

KOSNIK, M. A., HUA, Q., KAUFMAN, D. S. and WÜST, R. A. 2009. Taphonomic bias and time-averaging in tropical molluscan death assemblages: differential shell half-lives in Great Barrier Reef sediment. *Paleobiology*, **35**, 565–586.

KOWALEWSKI, M., DULAI, A. and FURSICH, F. T. 1998. A fossil record full of holes: the Phanerozoic history of drilling predation. *Geology*, **26**, 1091–1094.

KRAUSE, R. A., BARBOUR, S. L., KOWALEWSKI, M., KAUFMAN, D. S., ROMANEK, C. S., SIMÕES, M. G. and WEHMILLER, J. F. 2010. Quantitative comparisons and models of time-averaging in bivalve and brachiopod shell accumulations. *Paleobiology*, **36**, 428–452.

LAZO, D. G. 2004. Bivalve taphonomy: testing the effect of life habits on the shell condition of the littleneck clam *Protothaca* (*Protothaca*) *staminea* (Mollusca: Bivalvia). *PALAIOS*, **19**, 451–459.

LE, J. and SHACKLETON, N. J. 1992. Carbonate dissolution fluctuations in the western equatorial Pacific during the late Quaternary. *Paleoceanography*, **7**, 21–42.

LEE, J. H., HONG, J., LEE, D. J. and CHOH, S. J. 2016. A new Middle Ordovician bivalve–siliceous sponge–microbe reef-building consortium from North China. *Palaeogeography, Palaeoclimatology, Palaeoecology*, **457**, 23–30.

LI, F., QU, X., DU, L., DAI, T., YANG, Y., LI, J. and YANG, C. 2016. Genetic processes and environmental significance of Lower Devonian brachiopod shell concentrations in Longmenshan area, Sichuan, China. *Journal of Asian Earth Sciences*, **115**, 393–403.

LLOMPART, C. 1988. Braquiópodos del Banco de Chella (Mar de Alborán, Mediterráneo Occidental). *Acta Geologica Hispánica*, **23**, 311–319.

MANOJLOVIC, M. and CLAPHAM, M. E. 2021. The role of bioturbation-driven substrate disturbance in the Mesozoic brachiopod decline. *Paleobiology*, **47**, 86–100.

MARANO, G., UNGARO, N. and VACCARELLA, R. 1989. Nota preliminare sulle comunità di macroinvertebrati dei fondi strascicabili dell'Adriatico pugliese. *Thalassia Salentina*, **19**, 3–19.

MARGOLIN, A. R., ROBINSON, L. F., BURKE, A., WALLER, R. G., SCANLON, K. M., ROBERTS, M. L., AURO, M. E. and VAN DE FLIERDT, T. 2014. Temporal and spatial distributions of cold-water corals in the Drake Passage: insights from the last 35,000 years. *Deep Sea Research Part II: Topical Studies in Oceanography*, **99**, 237–248.

MARTIN, R. E. and SERVAIS, T. 2020. Did the evolution of the phytoplankton fuel the diversification of the marine biosphere? *Lethaia*, **53**, 5–31.

MEILE, C. and CAPPELLEN, P. V. 2003. Global estimates of enhanced solute transport in marine sediments. *Limnology & Oceanography*, **48**, 777–786.

MEKIK, F. A., LOUBERE, P. W. and ARCHER, D. E. 2002. Organic carbon flux and organic carbon to calcite flux ratio recorded in deep-sea carbonates: demonstration and a new proxy. *Global Biogeochemical Cycles*, **16**, 1052.

MERGL, M. 2020. Dendritic microborings in brachiopod shells from the Silurian of the Barrandian area, Czech Republic. *Bulletin of Geosciences*, **95**, 313–332.

MESSINA, C. and LABARBERA, M. 2004. Hydrodynamic behavior of brachiopod shells: experimental estimates and field observations. *PALAIOS*, **19**, 441–450.

MIDDELBURG, J. J., SOETAERT, K. and HERMAN, P. M. 1997. Empirical relationships for use in global diagenetic models. *Deep Sea Research Part I: Oceanographic Research Papers*, **44**, 327–344.

NAWROT, R., BERENSMEIER, M., GALLMETZER, I., HASELMAIR, A., TOMAŠOVÝCH, A. and ZUSCHIN, M. 2022. Multiple phyla, one time resolution? Similar time averaging in benthic foraminifera, mollusk, echinoid, crustacean and otolith fossil assemblages. *Geology*, **50**, 902–906.

NEUMANN, C., WISSHAK, M., ABERHAN, M., GIROD, P., RÖSNER, T. and BROMLEY, R. G. 2014. *Centrichnus eccentricus* revisited: a new view on anomiid bivalve bioerosion. *Acta Palaeontologica Polonica*, **60**, 539–549.

NOBLE, J. P. A. and LOGAN, A. 1981. Size-frequency distributions and taphonomy of brachiopods: a recent model. *Palaeogeography, Palaeoclimatology, Palaeoecology*, **36**, 87–105.

NOÉ, S., TITSCHACK, J., FREIWALD, A. and DULLO, W. C. 2006. From sediment to rock: diagenetic processes of hardground formation in deep-water carbonate mounds of the NE Atlantic. *Facies*, **52**, 183–208.

OLSZEWSKI, T. 1999. Taking advantage of time-averaging. *Paleobiology*, **25**, 226–238.

OLSZEWSKI, T. D. and KAUFMAN, D. S. 2015. Tracing burial history and sediment recycling in a shallow estuarine setting (Copano Bay, Texas) using post-mortem ages of the bivalve *Mulinia lateralis*. *PALAIOS*, **30**, 224–237.

PACE, S. M., POUSSARD, L. M., POWELL, E. N., ASHTON-ALCOX, K. A., KUYKENDALL, K. M., SOLINGER, L. K., HEMEON, K. M. and SONIAT, T. M. 2020. Dying, decaying, and dissolving into irrelevance: first direct in-the-field estimate of *Crassostrea virginica* shell loss—a case history from Mississippi Sound. *Journal of Shellfish Research*, **39**, 245–256.

PANETTA, P., MASTROTOTARO, F., CHIMIENTI, G., ANGELETTI, L. and D'ONGHIA, G. 2013. Tanatocenosi Wurmiana nel Canyon di Bari (Mar Adriatico). *Biologia Marina Mediterranea*, **20**, 148–149.

PARK, J., LEE, J. H., HONG, J., CHOH, S. J., LEE, D. C. and LEE, D. J. 2017. Crouching shells, hidden sponges: unusual Late Ordovician cavities containing sponges. *Sedimentary Geology*, **347**, 1–9.

PARSONS-HUBBARD, K. M., CALLENDER, W. R., POWELL, E. N., BRETT, C. E., WALKER, S. E., RAYMOND, A. L. and STAFF, G. M. 1999. Rates of burial and disturbance of experimentally-deployed molluscs; implications for preservation potential. *PALAIOS*, **14**, 337–351.

PETSIOS, E., PORTELL, R. W., FARRAR, L., TENNAKOON, S., GRUN, T. B., KOWALEWSKI, M. and TYLER, C. L. 2021. An asynchronous Mesozoic marine revolution: the Cenozoic intensification of predation on echinoids. *Proceedings of the Royal Society B*, **288**, 20210400.

POWELL, E. N. 1992. A model for death assemblage formation: can sediment shelliness be explained? *Journal of Marine Research*, **50**, 229–265.

POWELL, E. N., KRAEUTER, J. N. and ASHTON-ALCOX, K. A. 2006. How long does oyster shell last on an oyster reef? *Estuarine, Coastal & Shelf Science*, **69**, 531–542.

POWELL, E. N., BRETT, C. E., PARSONS-HUBBARD, K. M., CALLENDER, W. R., STAFF, G. M., WALKER, S. E., RAYMOND, A. and ASHTON-ALCOX, K. A. 2011*a*. The relationship of bionts and taphonomic processes in molluscan taphofacies formation on the continental shelf and slope: eight-year trends: Gulf of Mexico and Bahamas. *Facies*, **57**, 15–37.

POWELL, E. N., STAFF, G. M., CALLENDER, W. R., ASHTON-ALCOX, K. A., BRETT, C. E., PARSONS-HUBBARD, K. M., WALKER, S. E. and RAYMOND, A. 2011*b*. Taphonomic degradation of molluscan remains during thirteen years on the continental shelf and slope of the northwestern Gulf of Mexico. *Palaeogeography, Palaeoclimatology, Palaeoecology*, **312**, 209–232.

PRAMPOLINI, M., ANGELETTI, L., CASTELLAN, G., GRANDE, V., LE BAS, T., TAVIANI, M. and FOGLINI, F. 2021. Benthic habitat map of the southern adriatic sea (Mediterranean Sea) from object-based image analysis of multisource acoustic backscatter data. *Remote Sensing*, **13**, 2913.

PRATT, N., CHEN, T., LI, T., WILSON, D. J., VAN DE FLIERDT, T., LITTLE, S. H., TAYLOR, M. L.,

ROBINSON, L. F., ROGERS, A. D. and SANTODOMINGO, N. 2019. Temporal distribution and diversity of cold-water corals in the southwest Indian Ocean over the past 25,000 years. *Deep Sea Research Part I: Oceanographic Research Papers*, **149**, 103049.

PRÉAT, A., MORANO, S., LOREAU, J. L., DURLET, C. and MAMET, B. 2006. Petrography and biosedimentology of the Rosso Ammonitico Veronese (middle-upper Jurassic, north-eastern Italy). *Facies*, **52**, 265–278.

PRUDEN, M. J., MENDONCA, S. E. and LEIGHTON, L. R. 2018. The effects of predation on the preservation of ontogenetically young individuals. *Palaeogeography, Palaeoclimatology, Palaeoecology*, **490**, 404–414.

RADLEY, J. D. 2010. Grazing bioerosion in Jurassic seas: a neglected factor in the Mesozoic marine revolution? *Historical Biology*, **22**, 387–393.

REIMER, P. J. and McCORMAC, F. G. 2002. Marine radiocarbon reservoir corrections for the Mediterranean and Aegean Seas. *Radiocarbon*, **44**, 159–166.

REIMERS, C. E., JAHNKE, R. A. and McCORKLE, D. C. 1992. Carbon fluxes and burial rates over the continental slope and rise off central California with implications for the global carbon cycle. *Global Biogeochemical Cycles*, **6**, 199–224.

REMIA, A. and TAVIANI, M. 2005. Shallow-buried Pleistocene *Madrepora*-dominated coral mounds on a muddy continental slope, Tuscan Archipelago, NE Tyrrhenian Sea. *Facies*, **50**, 419–425.

REOLID, M., GARCÍA-GARCÍA, F., TOMAŠOVÝCH, A. and SORIA, J. M. 2012. Thick brachiopod shell concentrations from prodelta and siliciclastic ramp in a Tortonian Atlantic–Mediterranean strait (Miocene, Guadix Basin, southern Spain). *Facies*, **58**, 549–571.

RIDENTE, D., FOGLINI, F., MINISINI, D., TRINCARDI, F. and VERDICCHIO, G. 2007. Shelf-edge erosion, sediment failure and inception of Bari Canyon on the Southwestern Adriatic Margin (Central Mediterranean). *Marine Geology*, **246**, 193–207.

RITTER, M. D. N., ERTHAL, F., KOSNIK, M. A., COIMBRA, J. C. and KAUFMAN, D. S. 2017. Spatial variation in the temporal resolution of subtropical shallow-water molluscan death assemblages: spatial variation in time-averaging. *PALAIOS*, **32**, 572–583.

RIVERS, J. M., JAMES, N. P., KYSER, T. K. and BONE, Y. 2007. Genesis of palimpsest cool-water carbonate sediment on the continental margin of southern Australia. *Journal of Sedimentary Research*, **77**, 480–494.

RODLAND, D. L., KOWALEWSKI, M., CARROLL, M. and SIMÕES, M. G. 2006. The temporal resolution of epibiont assemblages: are they ecological snapshots or overexposures? *Journal of Geology*, **114**, 313–324.

RODLAND, D. L., SIMÕES, M. G., KRAUSE, R. A. Jr. and KOWALEWSKI, M. 2014. Stowing away on ships that pass in the night: sclerobiont assemblages on individually dated bivalve and brachiopod shells from a subtropical shelf. *PALAIOS*, **29**, 170–183.

RODRIGUES, S. C. 2007. Biotic interactions recorded in shells of recent rhynchonelliform brachiopods from San Juan Island, USA. *Journal of Shellfish Research*, **26**, 241–252.

RODRIGUES, S. C. and SIMÕES, M. G. 2010. Taphonomy of *Bouchardia rosea* (Rhynchonelliformea, Brachiopoda) shells from Ubatuba Bay, Brazil: implications for the use of taphonomic signatures in (paleo)environmental analysis. *Ameghiniana*, **47**, 373–386.

RODRIGUES, S. C., SIMÕES, M. G., KOWALEWSKI, M., PETTI, M. A., NONATO, E. F., MARTINEZ, S. and DEL RIO, C. J. 2008. Biotic interaction between spionid polychaetes and bouchardiid brachiopods: paleoecological, taphonomic and evolutionary implications. *Acta Palaeontologica Polonica*, **53**, 657–668.

ROSSO, A., VERTINO, A., DI GERONIMO, I., SANFILIPPO, R., SCIUTO, F., DI GERONIMO, R., VIOLANTI, D., CORSELLI, C., TAVIANI, M., MASTROTOTARO, F. and TURSI, A. 2010. Hard-and soft-bottom thanatofacies from the Santa Maria di Leuca deep-water coral province, Mediterranean. *Deep Sea Research Part II: Topical Studies in Oceanography*, **57**, 360–379.

RUGGIERO, E. T. and RAIA, P. 2010. Bioerosion structures and their distribution on shells of the Lower Pleistocene terebratulid brachiopod *Gryphus minor*. *Palaeogeography, Palaeoclimatology, Palaeoecology*, **293**, 157–166.

SALAMON, M. A., NIEDŹWIEDZKI, R., GORZELAK, P., LACH, R. and SURMIK, D. 2012. Bromalites from the Middle Triassic of Poland and the rise of the Mesozoic Marine Revolution. *Palaeogeography, Palaeoclimatology, Palaeoecology*, **321**, 142–150.

SANFILIPPO, R., VERTINO, A., ROSSO, A., BEUCK, L., FREIWALD, A. and TAVIANI, M. 2013. Serpula aggregates and their role in deep-sea coral communities in the southern Adriatic Sea. *Facies*, **59**, 663–677.

SCHWEITZER, C. E. and FELDMANN, R. M. 2010. The Decapoda (Crustacea) as predators on Mollusca through geologic time. *PALAIOS*, **25**, 167–182.

SEILACHER, A. 1968. Sedimentationsprozesse im Ammonitengehausen. *Akademie der Wissenschaften und der Literatur zu Mainz, Abhandlungen der mathematisch-naturwissenschaftlichen Klasse*, **1967**, 191–203.

SHEEHAN, P. M. 1978. The hinging mechanisms of brachiopods—taphonomic considerations. *Journal of Paleontology*, **52**, 748.

SIMÕES, M. G., KOWALEWSKI, M., TORELLO, F. F., GHILARDI, R. P. and MELLO, L. H. C. 2000. Early onset of modern-style shell beds in the Permian sequences of the Paraná Basin: implications for the Phanerozoic trend in bioclastic accumulations. *Revista Brasileira de Geociências*, **30**, 495–499.

SIMÕES, M. G., RODRIGUES, S. C., LEME, J. D. M. and JÚNIOR, M. C. B. 2005. The settling pattern of brachiopod shells: stratigraphic and taphonomic implications to shell bed formation and paleoecology. *Brazilian Journal of Geology*, **35**, 383–391.

SIMÕES, M. G., RODRIGUES, S. C., DE MORAES LEME, J. and PIRES-DOMINGUES, R. A. 2007*a*. Brachiopod shells on the beach: taphonomic overprinting in a fair-weather shell accumulation. *Journal of Taphonomy*, **5**, 205–225.

SIMÕES, M. G., RODRIGUES, S. C. and KOWALEWSKI, M. 2007*b*. Comparative analysis of drilling

frequencies in recent brachiopod-mollusk associations from the southern Brazilian shelf. *PALAIOS*, **22**, 143–154.

SIMÕES, M. G., RODRIGUES, S. C. and KOWALEWSKI, M. 2009. *Bouchardia rosea*, a vanishing brachiopod species of the Brazilian platform: taphonomy, historical ecology and conservation paleobiology. *Historical Biology*, **21**, 123–137.

ŠIMUNOVIĆ, A. 1997. Quantitative and qualitative investigations of benthic communities in the areas of mobile bottoms of the Adriatic Sea. *Acta Adriatica*, **38**, 77–194.

SKOMPSKI, S., BALIŃSKI, A., SZULCZEWSKI, M. and ZAWADZKA, I. 2018. Middle/Upper Devonian brachiopod shell concentrations from the intra-shelf basinal carbonates of the Holy Cross Mountains (central Poland). *Acta Geologica Polonica*, **68**, 607–633.

SMITH, C. R., LEVIN, L. A., HOOVER, D. J., McMURTRY, G. and GAGE, J. D. 2000. Variations in bioturbation across the oxygen minimum zone in the northwest Arabian Sea. *Deep Sea Research Part II: Topical Studies in Oceanography*, **47**, 227–257.

STURANY, R. 1896. Zoologische Ergebnisse. VIII. Brachiopoden, gesammelt auf den Expeditionen SM Schiffes "Pola" 1890–1894. *Denkschriften der Kaiserliche Akademie der Wissenschaften in Wien*, **63**, 37–38.

SUÁREZ-IBARRA, J. Y., FROZZA, C. F., PETRÓ, S. M. and PIVEL, M. A. G. 2021. Fragment or broken? Improving the planktonic foraminifera fragmentation assessment. *PALAIOS*, **36**, 165–172.

SUCHÉRAS-MARX, B., MATTIOLI, E., ALLEMAND, P., GIRAUD, F., PITTET, B., PLANCQ, J. and ESCARGUEL, G. 2019. The colonization of the oceans by calcifying pelagic algae. *Biogeosciences*, **16**, 2501–2510.

TACKETT, L. S. and TINTORI, A. 2019. Low drilling frequency in Norian benthic assemblages from the southern Italian Alps and the role of specialized durophages during the Late Triassic. *Palaeogeography, Palaeoclimatology, Palaeoecology*, **513**, 25–34.

TADDEI RUGGIERO, E. and BITNER, M. A. 2007. Bioerosion on brachiopod shells – a Cenozoic perspective. *Earth & Environmental Science Transactions of the Royal Society of Edinburgh*, **98**, 369–378.

TAVIANI, M. 1978. Associazioni a Molluschi pleistoceniche-attuali dragate nell'Adriatico meridionale. *Italian Journal of Zoology*, **45**, 297–306.

TAVIANI, M., ANGELETTI, L., BEUCK, L., CAMPIANI, E., CANESE, S., FOGLINI, F., FREIWALD, A., MONTAGNA, P. and TRINCARDI, F. 2016. Reprint of 'On and off the beaten track: Megafaunal sessile life and Adriatic cascading processes'. *Marine Geology*, **375**, 146–160.

TAVIANI, M., ANGELETTI, L., FOGLINI, F., CORSELLI, C., NASTO, I., PONS-BRANCHU, E. and MONTAGNA, P. 2019. U/Th dating records of cold-water coral colonization in submarine canyons and adjacent sectors of the southern Adriatic Sea since the Last Glacial Maximum. *Progress in Oceanography*, **175**, 300–308.

TESI, T., LANGONE, L., GONI, M. A., TURCHETTO, M., MISEROCCHI, S. and BOLDRIN, A. 2008. Source and composition of organic matter in the Bari canyon (Italy): dense water cascading versus particulate export from the upper ocean. *Deep Sea Research Part I: Oceanographic Research Papers*, **55**, 813–831.

TESI, T., ASIOLI, A., MINISINI, D., MASELLI, V., DALLA VALLE, G., GAMBERI, F., LANGONE, L., CATTANEO, A., MONTAGNA, P. and TRINCARDI, F. 2017. Large-scale response of the Eastern Mediterranean thermohaline circulation to African monsoon intensification during sapropel S1 formation. *Quaternary Science Reviews*, **159**, 139–154.

TESSITORE, L., SCHEMM-GREGORY, M., KORN, D., WILD, F. R., NAGLIK, C. and KLUG, C. 2013. Taphonomy and palaeoecology of the green Devonian gypidulid brachiopods from the Aferdou El Mrakib, eastern Anti-Atlas, Morocco. *Swiss Journal of Palaeontology*, **132**, 23–44.

THAMDRUP, B., GLUD, R. N. and HANSEN, J. W. 1994. Manganese oxidation and in situ manganese fluxes from a coastal sediment. *Geochimica et Cosmochimica Acta*, **58**, 2563–2570.

THAYER, C. W. 1983. Sediment-mediated biological disturbance and the evolution of marine benthos. 479–625. *In* TEVESZ, M. J. S. and McCALL, P. L. (eds) *Biotic interactions in recent and fossil benthic communities*. Topics in Geobiology, **3**. Springer.

THIAGARAJAN, N., GERLACH, D., ROBERTS, M. L., BURKE, A., McNICHOL, A., JENKINS, W. J., SUBHAS, A. V., THRESHER, R. E. and ADKINS, J. F. 2013. Movement of deep-sea coral populations on climatic timescales. *Paleoceanography*, **28**, 227–236.

THRESHER, R. E., TILBROOK, B., FALLON, S., WILSON, N. C. and ADKINS, J. 2011*a*. Effects of chronic low carbonate saturation levels on the distribution, growth and skeletal chemistry of deep-sea corals and other seamount megabenthos. *Marine Ecology Progress Series*, **442**, 87–99.

THRESHER, R. E., ADKINS, J. and THIAGARAJAN, N. 2011*b*. Modal analysis of the deep-water solitary scleractinian, *Desmophyllum dianthus*, on SW Pacific seamounts: inferred recruitment periodicity, growth, and mortality rates. *Coral Reefs*, **30**, 1063–1070.

THUNELL, R. C. 1976. Optimum indices of calcium carbonate dissolution, in deep-sea sediments. *Geology*, **4**, 525–528.

TOMAŠOVÝCH, A. 2004. Postmortem durability and population dynamics affecting the fidelity of brachiopod size-frequency distributions. *PALAIOS*, **19**, 477–496.

TOMAŠOVÝCH, A. 2008. Substrate exploitation and resistance to biotic disturbance in the brachiopod *Terebratalia transversa* and the bivalve *Pododesmus macrochisma*. *Marine Ecology Progress Series*, **363**, 157–170.

TOMAŠOVÝCH, A. and KIDWELL, S. M. 2017. Nineteenth-century collapse of a benthic marine ecosystem on the open continental shelf. *Proceedings of the Royal Society B*, **284**, 20170328.

TOMAŠOVÝCH, A. and ROTHFUS, T. 2005. Differential taphonomy of modern brachiopods (San Juan Islands, Washington State): effect of intrinsic factors on damage and community-level abundance. *Lethaia*, **38**, 271–292.

TOMAŠOVÝCH, A. and ZUSCHIN, M. 2009. Variation in brachiopod preservation along a carbonate shelf-basin transect (Red Sea and Gulf of Aden): environmental sensitivity of taphofacies. *PALAIOS*, **24**, 697–716.

TOMAŠOVÝCH, A., FÜRSICH, F. T. and WILMSEN, M. 2006. Preservation of autochthonous shell beds by positive feedback between increased hardpart-input rates and increased sedimentation rates. *Journal of Geology*, **114**, 287–312.

TOMAŠOVÝCH, A., KIDWELL, S. M., BARBER, R. F. and KAUFMAN, D. S. 2014. Long-term accumulation of carbonate shells reflects a 100-fold drop in loss rate. *Geology*, **42**, 819–822.

TOMAŠOVÝCH, A., KIDWELL, S. M. and BARBER, R. F. 2016*a*. Inferring skeletal production from time-averaged assemblages: skeletal loss pulls the timing of production pulses towards the modern period. *Paleobiology*, **42**, 54–76.

TOMAŠOVÝCH, A., SCHLÖGL, J., KAUFMAN, D. S. and HUDÁČKOVÁ, N. 2016*b*. Temporal and bathymetric resolution of nautiloid death assemblages in stratigraphically condensed oozes (New Caledonia). *Terra Nova*, **28**, 271–278.

TOMAŠOVÝCH, A., GALLMETZER, I., HASELMAIR, A., KAUFMAN, D. S., KRALJ, M., CASSIN, D., ZONTA, R. and ZUSCHIN, M. 2018. Tracing the effects of eutrophication on molluscan communities in sediment cores: outbreaks of an opportunistic species coincide with reduced bioturbation and high frequency of hypoxia in the Adriatic Sea. *Paleobiology*, **44**, 575–602.

TOMAŠOVÝCH, A., ALBANO, P. G., FUKSI, T., GALLMETZER, I., HASELMAIR, A., KOWALEWSKI, M., NAWROT, R., NERLOVIĆ, V., SCARPONI, D. and ZUSCHIN, M. 2020. Ecological regime shift preserved in the Anthropocene stratigraphic record. *Proceedings of the Royal Society B*, **287**, 20200695.

TOMAŠOVÝCH, A., BERENSMEIER, M., GALLMETZER, I., HASELMAIR, A. and ZUSCHIN, M. 2021. Pyrite-lined shells as indicators of inefficient bioirrigation in the Holocene–Anthropocene stratigraphic record. *Biogeosciences*, **18**, 5929–5965.

TOMAŠOVÝCH, A., GARCÍA-RAMOS, D., NAWROT, R., NEBELSICK, J. H. and ZUSCHIN, M. 2022*a*. Millennial-scale changes in abundance of brachiopods in bathyal environments detected by postmortem age distributions in death assemblage (Bari Canyon, Adriatic Sea). *Geological Society of London, Special Publications*, **529**, 117.

TOMAŠOVÝCH, A., GARCÍA-RAMOS, D. A., NAWROT, R., NEBELSICK, J. H. and ZUSCHIN, M. 2022*b*. Data from: How long does a brachiopod shell last on a seafloor? Modern mid-bathyal environments as taphonomic analogues of continental shelves prior to the Mesozoic Marine Revolution. *Dryad Digital Repository*. https://doi.org/10.5061/dryad.8w9ghx3qb

TOMAŠOVÝCH, A., GALLMETZER, I., HASELMAIR, A. and ZUSCHIN, M. 2022*c*. Inferring time averaging and hiatus durations in the stratigraphic record of high-frequency depositional sequences. *Sedimentology*, **69**, 1083–1118.

TRINCARDI, F., FOGLINI, F., VERDICCHIO, G., ASIOLI, A., CORREGGIARI, A., MINISINI, D., PIVA, A., REMIA, A., RIDENTE, D. and TAVIANI, M. 2007*a*. The impact of cascading currents on the Bari Canyon System, SW-Adriatic margin (Central Mediterranean). *Marine Geology*, **246**, 208–230.

TRINCARDI, F., VERDICCHIO, G. and MISEROCCHI, S. 2007*b*. Seafloor evidence for the interaction between cascading and along-slope bottom water masses. *Journal of Geophysical Research*, **112**, F03011.

TRINCARDI, F., ARGNANI, A. and CORREGGIARI, A., 2011. Note illustrative della Carta Geologica dei Mari Italiani, alla scala 1 a 250000. Foglio NK33-6 Vieste, e Foglio NK33-8/9 Bari, 1-194.

TURCHETTO, M., BOLDRIN, A., LANGONE, L., MISEROCCHI, S., TESI, T. and FOGLINI, F. 2007. Particle transport in the Bari canyon (southern Adriatic Sea). *Marine Geology*, **246**, 231–247.

USUI, A., HINO, H., SUZUSHIMA, D., TOMIOKA, N., SUZUKI, Y., SUNAMURA, M., KATO, S., KASHIWABARA, T., KIKUCHI, S., URAMOTO, G. I. and SUZUKI, K. 2020. Modern precipitation of hydrogenetic ferromanganese minerals during on-site 15-year exposure tests. *Scientific Reports*, **10**, 3558.

VERDICCHIO, G., TRINCARDI, F. and ASIOLI, A. 2007. Mediterranean bottom-current deposits: an example from the Southwestern Adriatic Margin. *Geological Society, London, Special Publications*, **276**, 199–224.

WALKER, S. E. and BRETT, C. E. 2002. Post-Paleozoic patterns in marine predation: was there a Mesozoic and Cenozoic marine predatory revolution? *Paleontological Society Papers*, **8**, 119–194.

WALKER, S. E., PARSONS-HUBBARD, K., POWELL, E. N. and BRETT, C. E. 1998. Bioerosion or bioaccumulation? Shelf-slope trends for epi-and endobionts on experimentally deployed gastropod shells. *Historical Biology*, **13**, 61–72.

WALKER, S. E., PARSONS-HUBBARD, K., POWELL, E. and BRETT, C. E. 2002. Predation on experimentally deployed molluscan shells from shelf to slope depths in a tropical carbonate environment. *PALAIOS*, **17**, 147–170.

WALKER, S. E., PARSONS-HUBBARD, K., RICHARDSON-WHITE, S., BRETT, C. and POWELL, E. 2011. Alpha and beta diversity of encrusting foraminifera that recruit to long-term experiments along a carbonate platform-to-slope gradient: paleoecological and paleoenvironmental implications. *Palaeogeography, Palaeoclimatology, Palaeoecology*, **312**, 325–349.

WALTER, L. M., BISCHOF, S. A., PATTERSON, W. P. and LYONS, T. W. 1993. Dissolution and recrystallization in modern shelf carbonates: evidence from pore water and solid phase chemistry. *Philosophical Transactions of the Royal Society A*, **344**, 27–36.

WETZEL, A. 2008. Recent bioturbation in the deep South China Sea: a uniformitarian ichnologic approach. *PALAIOS*, **23**, 601–615.

WISSHAK, M. 2017. Taming an ichnotaxonomical Pandora's box: revision of dendritic and rosetted microborings (ichnofamily: Dendrinidae). *European Journal of Taxonomy*, **390**, 1–99.

WISSHAK, M., GEKTIDIS, M., FREIWALD, A. and LUNDÄLV, T. 2005. Bioerosion along a bathymetric gradient in a cold-temperate setting (Kosterfjord, SW Sweden): an experimental study. *Facies*, **51**, 93–117.

ZONNEVELD, J. P. 2001. Middle Triassic biostromes from the Liard Formation, British Columbia, Canada: oldest examples from the Mesozoic of NW Pangea. *Sedimentary Geology*, **145**, 317–341.